Surg Today (2011) 41:1467–1474
DOI 10.1007/s00595-010-4553-0

SURGERY TODAY

Review Article

Assessing Intraoperative Blood Flow in Cardiovascular Surgery

MASAKI YAMAMOTO[1], SHIRO SASAGURI[1], and TAKAYUKI SATO[2]

Departments of [1]Surgery II and [2]Cardiovascular Control, Faculty of Medicine, Kochi University, Kohasu, Oko, Nankoku, Kochi 783-8505, Japan

Abstract
Off-pump coronary arterial bypass grafting and new surgical apparatus and techniques have decreased the mortality rate associated with this procedure to approximately 1.5%. If we could detect problems in the constructed coronary anastomoses by an alternative imaging system to coronary angiography during surgery, decisions to revise the surgical procedure could be made without hesitation. Meanwhile, the intraoperative direct evaluation of intestinal blood flow during abdominal aortic aneurysmal surgery is required to prevent ischemic colitis, which is a devastating complication. Indocyanine green (ICG) has recently improved ophthalmic angiography and the navigation systems of oncological surgery. The fluorescence illumination of ICG with a near-infrared light is captured on camera. In coronary arterial surgery, the ICG imaging system is also becoming increasingly useful. A new ICG imaging system, the HyperEye Medical System (HEMS), provides a clear view of the blood flow and ischemic area with color visualization. Furthermore, its combination with a quantitative blood flow assessment tool such as transit time flow measurement could improve the accuracy of intraoperative examination. In this review, we evaluate the current strategies of assessing blood flow intraoperatively with an ICG imaging system in cardiovascular surgery.

Key words Intraoperative assessment of blood flow · Indocyanine green imaging system · Hyper Eye Medical System · Coronary artery bypass grafting · Transit time flow measurement

Reprint requests to: M. Yamamoto
Received: August 24, 2010 / Accepted: November 17, 2010

Introduction

Coronary artery disease (CAD) has becomes the leading cause of death in developed countries. Surgery for angina and myocardial ischemia began with the Veinberg operation in 1946: Nowadays, about 18000 patients undergo coronary artery bypass grafting (CABG) each year in Japan. It has been reported that improved techniques, such as off-pump coronary artery bypass grafting (OPCAB), arterial grafts, and new surgical devices, have reduced the mortality of elective CABG down to about 1.5%.[1–4] The decreased mortality can also be attributed to advances in off-pump CABG; however, their effectiveness is dependent on surgical technique.[2,5–7] An increasing tendency toward re-CABG for recurrent angina attributed to graft occlusion or stenosis has been reported.[2] Balacumaraswami et al. reported 943 graft failures among 4735 grafts (19.9%) in patients who underwent CABG.[8]

The patency of bypass grafts has been evaluated with the coronary artery graph (CAG) and computed tomography (CT), while transit time flow measurement (TTFM) has also been introduced as an effective device for the intraoperative evaluation of bypass grafts.[9] Imaging techniques that rival CAG are required to allow us to see constructed coronary anastomoses. If problems with constructed coronary anastomoses can be detected through imaging as well as CAG during surgery, it would enable us to make a decision on revising the surgical procedure immediately. Furthermore, surgeons conventionally believe that it is difficult to identify the buried coronary artery that could be used in CABG anastomoses. Therefore, a detection tool is needed so we can decide which target coronary arteries should be bypass grafted.

Intestinal ischemia is a devastating complication of abdominal aortic aneurysm (AAA) repair, associated with a 40%–48% mortality rate.[10–12] Previously, the intestinal blood flow was assessed intraoperatively by mea-

suring inframesenteric artery (IMA) stump pressure, transanal Doppler ultrasound, and near-infrared spectroscopy. Ernst et al. prospectively studied the correlation between distal IMA stump pressure and ischemic colitis.[10] Ischemic colitis may develop after IMA or internal iliac artery (IIA) reconstruction.[12–14] The incidences of ischemic colitis after elective AAA surgery and AAA rupture are reported to be 6% and 42%, respectively.[12,13] According to Piotrowski et al., preoperative shock is the most important predictor of colonic ischemia following ruptured AAA.[15] Champagne et al. reported on the mortality rates of bowel ischemia with colonoscopic findings.[13] Although reconstruction of the blood flow in at least one IMA and IIA is commonly performed to prevent ischemic colitis, there is little evidence to support the effectiveness of these methods. Therefore, the direct evaluation of intestinal blood flow is required. Iwai et al. evaluated the rectal ischemia of patients who underwent AAA surgery by fixing a transanal Doppler probe in the rectum to detect blood flow in the upper rectal arterial area.[16] Furthermore, skin perfusion of both buttocks was detected with near-infrared spectroscopy. Visual evaluation of the intestinal blood flow intraoperatively allows us to decide on the need for reconstruction of the IMA or IIA in real time.

The incidence of peripheral artery occlusive disease (PAD) is increasing, for which catheter-based therapy is continually improving. The effectiveness of catheter-based therapy for PAD was demonstrated in a recent Bypass versus Angioplasty in Severe Ischemia of the Leg (BASIL) trial.[17] In the era of interventional surgery for PAD, the number of patients with critical limb ischemia requiring surgical therapy is substantially increasing. Although patients with the most advanced critical limb ischemia (CLI) should be given the choice of undergoing bypass involving either the tibial artery or the dorsal artery with saphenous vein grafts, anastomosis is often performed, despite the difficulties involved, because of the poor condition of the arteries.[17] It is common practice to evaluate the bypass graft with a portable X-ray fluoroscope or flowmetry during the operation. However, the use of conventional X-ray fluoroscope systems is associated with difficulties, such as complicated X-ray apparatus and establishing a line for angiography. Moreover, patients with chronic renal failure can suffer radiocontrast-induced renal failure. Technical errors when performing a bypass graft may necessitate lower limb amputation, limiting activities of daily living; therefore, a more reliable intraoperative imaging tool is required.

Intraoperative Imaging Techniques

Postoperative CAG and multidetector CT allow for visualization of anastomoses at a high resolution. Although these imaging tools enable us to detect problems with the graft postoperatively, it is too late to revise the graft anastomoses. Conversely, if the bypass graft patency and quality of anastomosis could be assessed intraoperatively, graft revision may be possible. Intraoperative indocyanine green (ICG) angiography would resolve this problem.[18–20]

Indocyanine Green Imaging

Indocyanine green is a hydrophilic tricarbocyanine dye that rapidly binds to plasma proteins in the body. It has been used for testing liver function and in ophthalmic angiography.[21] The fluorescence properties of ICG emit a flash of light with a wavelength of 806 nm, although our preliminary study showed that the peak spectral absorption for ICG diluted in human blood was 760–780 nm.[22] Water and hemoglobin have light absorption properties within organs. The fluorescence illuminated with near-infrared laser light or light-emitting diode (LED) light is captured on a charge-coupled device (CCD) video camera. Indocyanine green fluorescence illumination can be captured to a depth of less than 1 mm, allowing the visualization of blood flow in superficial tissues. The effectiveness of ICG angiography in fluorescein fundus angiography has improved the visualization of retinal and choroidal circulation.[23,24] The allergy-related reaction of ICG is dose dependent, being highest at a dose of more than 0.5 mg/kg body weight. This allergy-related reaction has been reported to occur at an incidence of approximately 1:40 000.[25]

Several reports have described a novel method of using ICG imaging to identify sentinel nodes with high sensitivity in breast and gastroenterological cancer.[26–28] In cardiovascular surgery, the value of intraoperative ICG imaging is being reported increasingly.[18,22,29,30] The commercialized SPY imaging system (Novadaq Technologies Inc., Toronto, Canada) is based on the fluorescence of ICG. The radiation of the SPY utilizes a low-intensity laser with a total output of 2.2 W spread over an area of 7.5 × 7.5 cm at a distance of 30 cm, which eliminates the risk of thermal injury.[29] In surgery, the articulating arm is covered with a sterile drape and after injecting ICG, the laser is activated and the image is acquired. A new ICG imaging system, the Photodynamic Eye (PDE; Hamamatsu Photonics K. K., Shizuoka, Japan), has been developed, which allows for imaging in the surgical field by using a hand-held camera. The PDE system is a simpler, more mobile, and improved version of the ICG imaging system.

HyperEye Medical System

We previously described a new ICG imaging system (HyperEye Medical System; HEMS, Mizuho Ikakogyo CO., Ltd, Japan) that consists of optical filters and an ultrahigh-sensitive color CCD imaging camera with

non-Bayer color filter arrays (HyperEye Technology; United States Patent Application 20080251694), which can detect visible and near-infrared rays from 380 to 1200 nm with no bias in the color balance, at 30 frames per second[22,31] (Fig. 1). Excitation of ICG is induced with an LED (760 nm) light source in the HEMS imaging system. The CCD camera is positioned about 30–50 cm above the surgical site. The focus, iris, and range are remote-controlled, thus ensuring that the camera is in a free position, and ICG dye is injected into the patient via a central venous catheter. The usual dose of ICG administered is 2.5 mg per image sequence. The video is recorded and stored immediately in AVI format, although the monochrome visualization of conventional ICG imaging cannot provide a surgical view on the monitor before the ICG injection. HEMS provides a different color image to conventional ICG imaging (Fig. 2). The color imaging recognizes the advantage of a navigation system in the orientation of the coronary arteries. Furthermore, in conventional ICG imaging that uses a laser light source, irradiation cannot be delivered for more than 35 s because of the danger of thermal injury. By contrast, the HEMS system provides color imaging without the problem of a limited irradiation time, by using LED.[22]

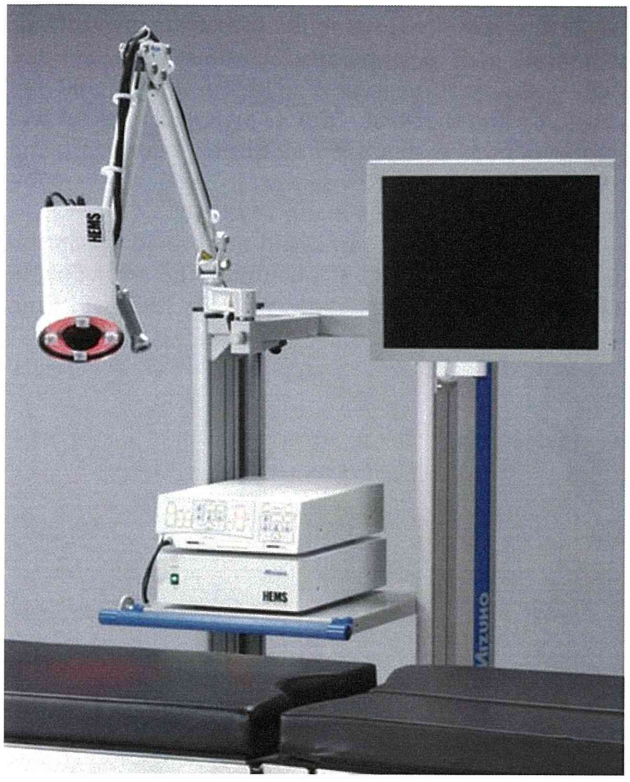

Fig. 1. The HyperEye Medical System (HEMS) consists of LED lights and an ultrasensitive color charge-coupled device (CCD) camera, which can visualize the optical wavelengths and near-infrared rays from 380 to 1200 nm

Transit Time Flow Measurement

Transit time flow measurement (TTFM) is based on the principle of transit time ultrasound technology.[32] The time it takes for ultrasound beams sent by an ultrasound wave to travel from one crystal across a vessel to the another crystal is called "transit time".[29,32] Blood flow such as that measured in a coronary arterial bypass graft, is rated by TTFM based on mean graft flow (MGF), pulsatility index (PI), and diastolic filling percentage (DF).[32–34] D'Ancona et al. explained that mean arterial blood pressure and graft coronary resistance influence mean flow.[32,33] They found that certain physical factors, such as blood viscosity, graft length, and graft radius, affect the aforementioned parameters.[32,33] Having studied the normal presented transit time patency criteria, the authors have set the following classification criteria, based on previous descriptions:[22]

Normal: mean flow >10 ml/min; PI <5; and DF >50%
Abnormal: mean flow <10 ml/min; PI >5; or DF <50%

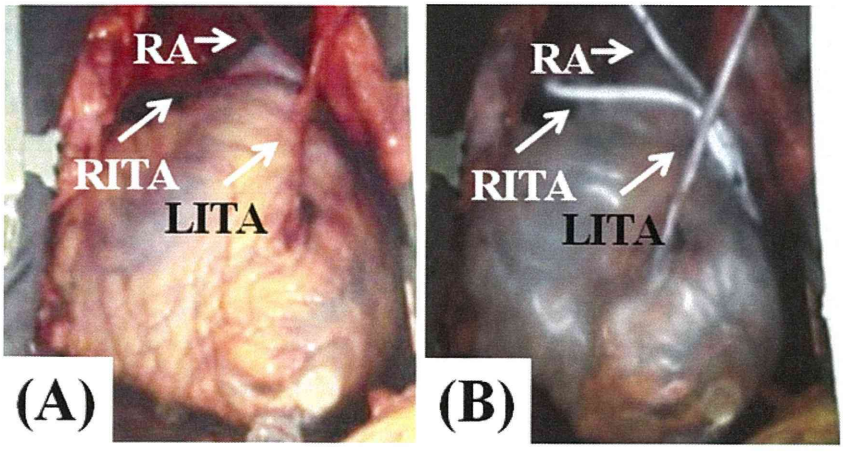

Fig. 2A,B. HEMS Indocyanine green (ICG) imaging shows the bypass graft and coronary arteries. The in situ left internal thoracic artery (*LITA*) was anastomosed to the left anterior descending artery, the right internal thoracic artery (*RITA*) was anastomosed to the diagonal branch, and the radial artery (*RA*) graft was anastomosed to the posterolateral coronary artery. **A** Pre-ICG imaging with a color-scale CCD HEMS. **B** The color-scale ICG imaging

If there is no quantifiable flow, a graft is deemed to be occluded.

Application of ICG Imaging in Cardiovascular Surgery

Usability of the ICG Imaging System in CABG

Since we can use the ICG imaging technique to assess the quality of coronary anastomoses visually, it allows us to decide on the need to revise anastomoses in real time (Fig. 3). Conversely, the prognosis of patients who do not undergo graft revision worsens if ICG imaging is not able to be done.[29] Other investigators have reported the reliability of intraoperative ICG imaging in clinical and experimental studies on CABG (Table 1). The first reported trial of intraoperative ICG imaging in coronary artery surgery was by Rubens et al. in 2002.[21] Reuthebuch et al.[19] and Taggart et al.[20] subsequently showed the clinical utility of the SPY system for assessing the quality of bypass grafts based on their experience. Takahashi et al. described the verification of ICG angiography by using the SPY imaging system.[18] In their study, the SPY system revealed four grafts problems among a collective 290 grafts in 72 off-pump CABG patients. Desai et al. researched the utility of two intraoperative graft assessment techniques: TTFM and ICG graft angiography.[35] They reviewed 139 grafts, and confirmed the sensitivity and specificity of ICG angiography by revealing that it detected greater than 50% stenosis or occlusion in 83.3% and 100%, respectively.[35] We have reported the reliability of ICG angiography as compared with postoperative coronary angiography. Fifth grafts were examined in this research, and the sensitivity and specificity of ICG angiography to detect greater than 50% stenosis or occlusion were 100% and 100%, respectively.[22] Revised graft anastomoses comprised 1.4% of all grafts in our research.

While ICG angiography could not provide quantitative measurements, TTFM quantified the graft flow in terms of certain parameters, such as MGF, PI, and

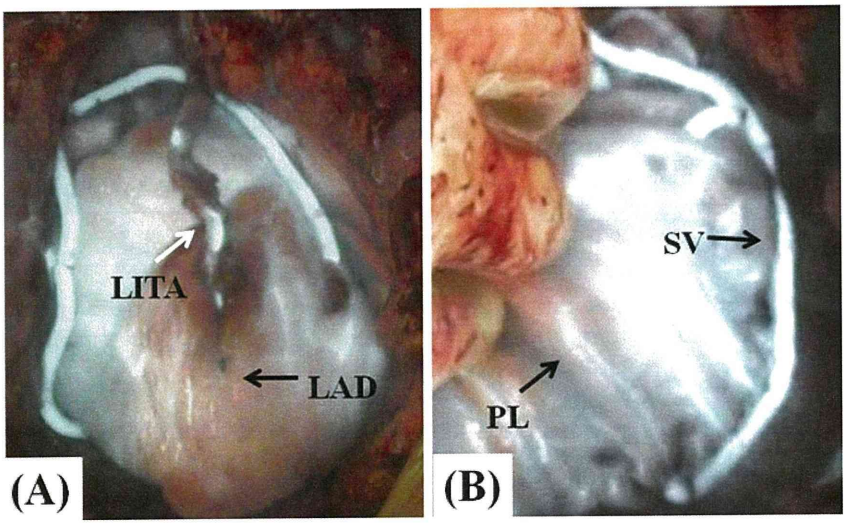

Fig. 3A,B. HEMS ICG imaging shows occlusion of the anastomosis of the left internal thoracic artery (*LITA*) graft to the left anterior descending artery (*LAD*). **A** No fluorescence was seen in the LITA graft to the LAD. There was no dye in the anterior wall of the left ventricle (the perfusion area of the LAD). **B** No fluorescence was seen in the saphenous vein (*SV*) graft to the posterolateral (*PL*) branch

Table 1. Reported clinical studies on the indocyanine green imaging system in coronary artery bypass grafting

First author[Ref.]	Year	Patients	No. of grafts	Sensitivity	Specificity
Rubens[21]	2002	20	—	—	—
Reuthebuch[19]	2003	38	124	—	—
Taggart[20]	2003	84	213	—	—
Balacumaraswami[29]	2004	200	533	—	—
Takahashi[18]	2004	72	290	—	—
Desai[35]	2006	46	139	83.3	100
Handa[22]	2009	39	116	100	100
Handa[31]	2010	51	129	85.7	100

—, not shown

DF.[8,19,32] The results of the intraoperative examination of TTFM have been documented by several institutions.[7,9,22,35,36] The results of clinical trials by Desai et al. showed that the sensitivity and specificity of TTFM in detecting greater than 50% stenosis or occlusion were 25% and 98.4%, respectively.[35] Hirotani et al. reported the utility of TTFM versus postoperative angiography.[7] In reviewing the clinical value of TTFM to assess graft patency, Balacumaraswami et al. reported that overall, 3.2% of 1411 grafts in 8.8% of 509 patients were revised according to TTFM findings.[29] However, based on their clinical studies, Balacumaraswami et al. suggested that TTFM findings alone may prompt unnecessary graft revision. D'Ancona et al. determined whether TTFM could be used to evaluate coronary graft patency in 409 patients who underwent CABG.[9] Of 1145 grafts, 37 (3.2%) were revised, 34 (3.0%) of which were revised for both low and abnormal flow curve patterns. In our recent studies, TTFM showed 5 competitive grafts among 116 grafts, although postoperative CAG showed that all the grafts were patent.[22,31] By contrast, CAG indicated graft failure in four grafts despite a normal flow pattern of TTFM, resulting in the sensitivity of TTFM being 93%.[22] Several intraoperative assessment modalities have been reported, including TTFM and ICG imaging, but it would not be possible to compare the advantages of ICG imaging and TTFM as their characteristics and methods are so different. Some investigators have compared the sensitivity and specificity of

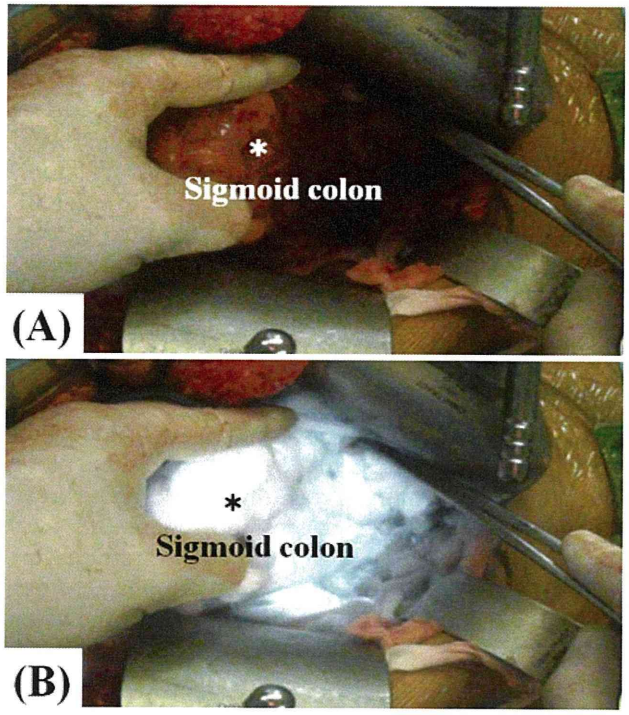

Fig. 4A,B. Indocyanine green fluorescence of the sigmoid colon (*asterisk*) in abdominal aneurysm surgery by HEMS ICG imaging. **A** Pre-ICG imaging of the sigmoid colon with a color-scale CCD camera. **B** Color-scale ICG imaging of the sigmoid colon

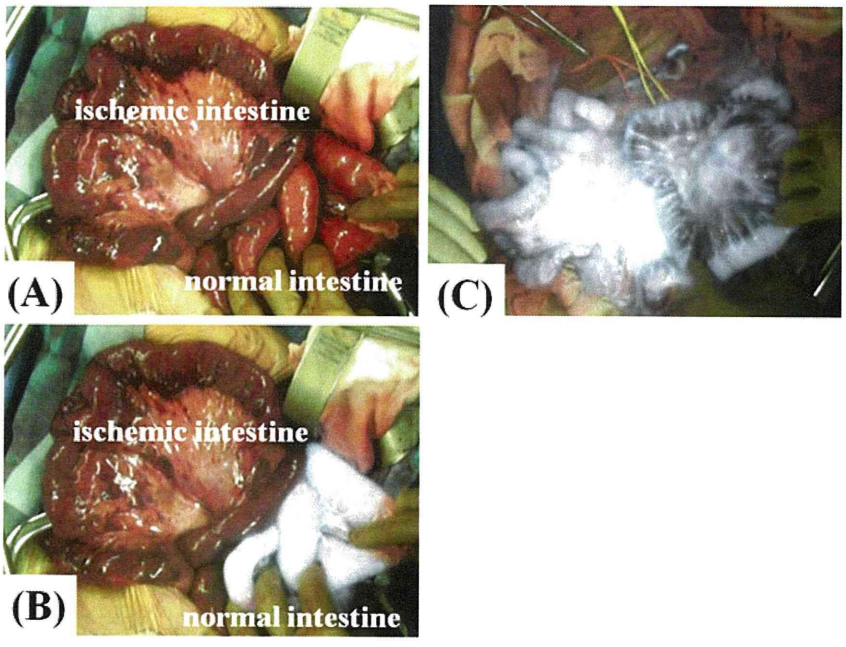

Fig. 5A–C. HEMS imaging showing intestine in the abdominal surgery. **A** Pre-ICG imaging with a color-scale CCD camera. **B** No fluorescence was seen in the ischemic intestine in the contrast of normal intestine. **C** After thrombectomy of the superior mesenteric artery, ICG imaging shows fluorescence in the reperfused intestine

ICG imaging with those of TTFM, but this comparison may not be useful. Indocyanine green imaging and TTFM are dependent to some degree on systemic blood pressure, cardiac output, hematocrit level, the variety and caliber of graft types, perfusion area, and ICG dosage. Therefore, these intraoperative assessment tools are unable to completely analyze the graft flow quantitatively. Both ICG imaging and TTFM can be used as intraoperative tools to assess graft flow in CABG. We believe that surgeons have no objection to either the use of or the comprehensive assessment of either tool.

Application in Vascular Surgery

By being able to visually assess intestinal blood flow intraoperatively, the need to reconstruct intestinal blood flow can be determined in real time. Indocyanine green imaging has been used to assess procedures for local perfusion in AAA surgery, similarly to the graft imaging used in CABG. In our study, HEMS color imaging allowed visualization of the ischemic area of the colon or intestine (Fig. 4). In principle, bilateral IIAs are reconstructed in our surgical strategy and IMA stump pressure is quantitatively evaluated in accordance with Ernst's procedure.[10] After this classical procedure, blood flow in the intestine and colon is confirmed by ICG imaging. HEMS color imaging allows us to pinpoint the exact location of the ischemic colon and the colored view helps us predict the obstruction point (Fig. 4). Moreover, abdominal organ ischemia is detected in real time during abdominal surgery, which is not the same as AAA surgery. We have experienced patients with a superior mesenteric arterial embolism. HEMS imaging allows us to detect the ischemic intestinal lesion and the thrombosed superior mesenteric artery (SMA) and its branches (Fig. 5). It also enables us to delineate the extent of ischemia from more than just a megascopic view.

Application in Peripheral Arterial Surgery

Digital subtraction angiography (DSA) with a portable X-ray machine is used for intraoperative imaging in peripheral arterial surgery. A mobile imaging system is also used for intraoperative imaging in PAD surgery. Unno et al. reported the clinical practicality of ICG imaging for assessing lower leg bypass with the PDE system in nine patients with CLI who underwent a distal bypass grafting.[37] ICG imaging using the PDE system showed that case graft revision was required in one patient when the initial bypass did not show any fluorescence signals at the distal anastomosis. We examined a CLI patient who underwent paramalleolar artery bypass. HEMS imaging showed a problem with the graft, and additional bypass grafting improved blood flow (Fig. 6).

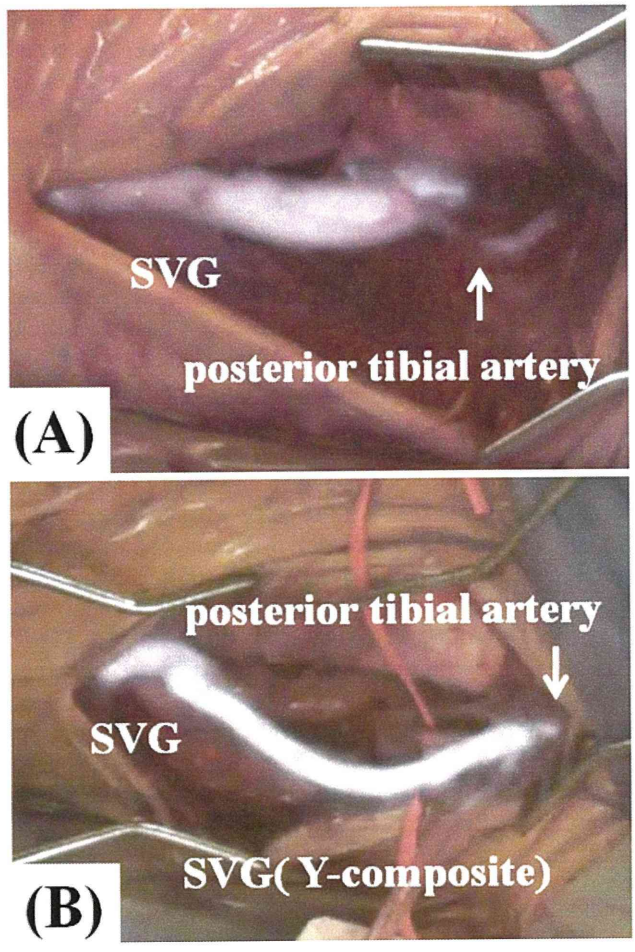

Fig. 6A,B. Indocyanine green imaging of a saphenous vein graft (*SVG*) in posterotibial arterial bypass. There was a lack of fluorescence in the posterior tibial artery

Indocyanine green imaging is useful in peripheral arterial surgery to assess graft patency quickly, with a high level of confidence. There is a great need for handheld ICG imaging systems, such as the PDE system, for broad-area imaging.

Conclusion

The ICG imaging system, which allows for visualization, has improved confidence in cardiovascular surgery and is used for graft assessment intraoperatively at many facilities. The HEMS allows the surgeon to see the blood flow clearly. If problems with constructed graft anastomoses can be evaluated through this type of imaging as well as angiography during surgery, decisions to revise the surgical procedure can be made without hesitation. Thus, in cardiovascular surgery, ICG imaging is a useful tool for evaluation of not only the coronary artery bypass, but also intestinal blood flow and the peripheral

arteries. It also enables us to detect signs of organ ischemia in real time. One of its limitations is that it cannot provide a quantitative evaluation of graft flow; however, TTFM allows for good quantitative assessment intraoperatively. Thus, the combination of ICG imaging and TTFM should be used for evaluation in cardiovascular surgery.

Acknowledgments. This study was supported by a grant for Science and Technology Incubation Program in Advanced Regions from the Japan Science and Technology Agency.

References

1. Parolari A, Alamanni F, Polvani G, Agrifoglio M, Chen YB, Kassem S, et al. Meta-analysis of randomized trials comparing off-pump with on-pump coronary artery bypass graft patency. Ann Thorac Surg 2005;80:2121–5.
2. Khan NE, De Souza A, Mister R, Flather M, Clague J, Davies S, et al. A randomized comparison of off-pump and on-pump multivessel coronary-artery bypass surgery. N Engl J Med 2004;350:21–8.
3. Puskas JD, Williams WH, Mahoney EM, Huber PR, Block PC, Duke PG, et al. Off-pump vs conventional coronary artery bypass grafting: early and 1-year graft patency, cost, and quality-of-life outcomes: a randomized trial. JAMA 2004;291:1841–9.
4. Shroyer AL, Grover FL, Hattler B, Collins JF, McDonald GO, Kozora E, et al. On-pump versus off-pump coronary-artery bypass surgery. N Engl J Med 2009;361:1827–37.
5. Puskas JD, Thourani VH, Marshall JJ, Dempsey SJ, Steiner MA, Sammons BH, et al. Clinical outcomes, angiographic patency, and resource utilization in 200 consecutive off-pump coronary bypass patients. Ann Thorac Surg 2001;71:1477–83; discussion 83–4.
6. Kobayashi J, Tashiro T, Ochi M, Yaku H, Watanabe G, Satoh T, et al. Early outcome of a randomized comparison of off-pump and on-pump multiple arterial coronary revascularization. Circulation 2005;112:I338–43.
7. Hirotani T, Kameda T, Shirota S, Nakao Y. An evaluation of the intraoperative transit time measurements of coronary bypass flow. Eur J Cardiothorac Surg 2001;19:848–52.
8. Balacumaraswami L, Taggart DP. Intraoperative imaging techniques to assess coronary artery bypass graft patency. Ann Thorac Surg 2007;83:2251–7.
9. D'Ancona G, Karamanoukian HL, Ricci M, Schmid S, Bergsland J, Salerno TA. Graft revision after transit time flow measurement in off-pump coronary artery bypass grafting. Eur J Cardiothorac Surg 2000;17:287–93.
10. Ernst CB, Hagihara PF, Daugherty ME, Griffen WO, Jr. Inferior mesenteric artery stump pressure: a reliable index for safe IMA ligation during abdominal aortic aneurysmectomy. Ann Surg 1978;187:641–6.
11. Chen JC, Hildebrand HD, Salvian AJ, Taylor DC, Strandberg S, Myckatyn TM, et al. Predictors of death in nonruptured and ruptured abdominal aortic aneurysms. J Vasc Surg 1996;24:614–20; discussion 21–3.
12. Champagne BJ, Lee EC, Valerian B, Mulhotra N, Mehta M. Incidence of colonic ischemia after repair of ruptured abdominal aortic aneurysm with endograft. J Am Coll Surg 2007;204:597–602.
13. Champagne BJ, Darling RC, 3rd, Daneshmand M, Kreienberg PB, Lee EC, Mehta M, et al. Outcome of aggressive surveillance colonoscopy in ruptured abdominal aortic aneurysm. J Vasc Surg 2004;39:792–6.
14. Zelenock GB, Strodel WE, Knol JA, Messina LM, Wakefield TW, Lindenauer SM, et al. A prospective study of clinically and endoscopically documented colonic ischemia in 100 patients undergoing aortic reconstructive surgery with aggressive colonic and direct pelvic revascularization, compared with historic controls. Surgery 1989;106:771–9; discussion 9–80.
15. Piotrowski JJ, Ripepi AJ, Yuhas JP, Alexander JJ, Brandt CP. Colonic ischemia: the Achilles heel of ruptured aortic aneurysm repair. Am Surg 1996;62:557–60; discussion 60–1.
16. Iwai T, Sakurazawa K, Sato S, Muraoka Y, Inoue Y, Endo M. Intraoperative monitoring of the pelvic circulation using a transanal Doppler probe. Euro J Vasc Surg 1991;5:71–4.
17. Conte MS. Bypass versus Angioplasty in Severe Ischaemia of the Leg (BASIL) and the (hoped for) dawn of evidence-based treatment for advanced limb ischemia. J Vasc Surg;51:69S–75S.
18. Takahashi M, Ishikawa T, Higashidani K, Katoh H. SPY: an innovative intra-operative imaging system to evaluate graft patency during off-pump coronary artery bypass grafting. Interact Cardiovasc Thorac Surg 2004;3:479–83.
19. Reuthebuch O, Haussler A, Genoni M, Tavakoli R, Odavic D, Kadner A, et al. Novadaq SPY: intraoperative quality assessment in off-pump coronary artery bypass grafting. Chest 2004;125:418–24.
20. Taggart DP, Choudhary B, Anastasiadis K, Abu-Omar Y, Balacumaraswami L, Pigott DW. Preliminary experience with a novel intraoperative fluorescence imaging technique to evaluate the patency of bypass grafts in total arterial revascularization. Ann Thorac Surg 2003;75:870–3.
21. Rubens FD, Ruel M, Fremes SE. A new and simplified method for coronary and graft imaging during CABG. Heart Surg Forum 2002;5:141–4.
22. Handa T, Katare RG, Sasaguri S, Sato T. Preliminary experience for the evaluation of the intraoperative graft patency with real color charge-coupled device camera system: an advanced device for simultaneous capturing of color and near-infrared images during coronary artery bypass graft. Interact Cardiovasc Thorac Surg 2009;9:150–4.
23. Piccolino FC, Borgia L, Zinicola E. Indocyanine green angiography of circumscribed choroidal hemangiomas. Retina 1996;16:19–28.
24. Flower RW, Hochheimer BF. A clinical technique and apparatus for simultaneous angiography of the separate retinal and choroidal circulations. Invest Ophthalmol 1973;12:248–61.
25. Kitai T, Miwa M, Liu H, Beauvoit B, Chance B, Yamaoka Y. Application of near-infrared time-resolved spectroscopy to rat liver — a preliminary report for surgical application. Phys Med Biol 1999;44:2049–61.
26. Kitai T, Inomoto T, Miwa M, Shikayama T. Fluorescence navigation with indocyanine green for detecting sentinel lymph nodes in breast cancer. Breast Cancer 2005;12:211–5.
27. Ohdaira H, Nimura H, Takahashi N, Mitsumori N, Kashiwagi H, Narimiya N, et al. The possibility of performing a limited resection and a lymphadenectomy for proximal gastric carcinoma based on sentinel node navigation. Surg Today 2009;39:1026–31.
28. Watanabe M, Tsunoda A, Narita K, Kusano M, Miwa M. Colonic tattooing using fluorescence imaging with light-emitting diode-activated indocyanine green: a feasibility study. Surg Today 2009;39:214–8.
29. Balacumaraswami L, Taggart DP. Digital tools to facilitate intraoperative coronary artery bypass graft patency assessment. Semin Thorac Cardiovasc Surg 2004;16:266–71.
30. Singh SK, Desai ND, Chikazawa G, Tsuneyoshi H, Vincent J, Zagorski BM, et al. The Graft Imaging to Improve Patency (GRIIP) clinical trial results. J Thorac Cardiovasc Surg;139:294–301.
31. Handa T, Katare RG, Nishimori H, Wariishi S, Fukutomi T, Yamamoto M, et al. New device for intraoperative graft assessment: HyperEye charge-coupled device camera system. Gen Thorac Cardiovasc Surg 2010;58:68–77.
32. D'Ancona G, Bartolozzi F, Bogers AJ, Pilato M, Parrinello M, Kappetein AP. Intraoperative graft patency verification in coro-

nary artery surgery: modern diagnostic tools. J Cardiothorac Vasc Anesth 2009;23:232–8.
33. Louagie YA, Haxhe JP, Jamart J, Buche M, Schoevaerdts JC. Doppler flow measurement in coronary artery bypass grafts and early postoperative clinical outcome. Thorac Cardiovasc Surg 1994;42:175–81.
34. Jaber SF, Koenig SC, BhaskerRao B, VanHimbergen DJ, Cerrito PB, Ewert DJ, et al. Role of graft flow measurement technique in anastomotic quality assessment in minimally invasive CABG. Ann Thorac Surg 1998;66:1087–92.
35. Desai ND, Miwa S, Kodama D, Koyama T, Cohen G, Pelletier MP, et al. A randomized comparison of intraoperative indocyanine green angiography and transit-time flow measurement to detect technical errors in coronary bypass grafts. J Thorac Cardiovasc Surg 2006;132:585–94.
36. Schmitz C, Ashraf O, Schiller W, Preusse CJ, Esmailzadeh B, Likungu JA, et al. Transit time flow measurement in on-pump and off-pump coronary artery surgery. J Thorac Cardiovasc Surg 2003;126:645–50.
37. Unno N, Suzuki M, Yamamoto N, Inuzuka K, Sagara D, Nishiyama M, et al. Indocyanine green fluorescence angiography for intraoperative assessment of blood flow: a feasibility study. Eur J Vasc Endovasc Surg 2008;35:205–7.

Nephrol Dial Transplant (2011) 26: 4023–4031
doi: 10.1093/ndt/gfr176
Advance Access publication 14 April 2011

Conditional *VHL* gene deletion activates a local NO–VEGF axis in a balanced manner reinforcing resistance to endothelium-targeted glomerulonephropathy

Taku Morita[1], Yoshihiko Kakinuma[2], Atsushi Kurabayashi[3], Mikiya Fujieda[1], Takayuki Sato[2], Taro Shuin[4], Mutsuo Furihata[3] and Hiroshi Wakiguchi[1]

[1]Department of Pediatrics, Kochi Medical School, Nankoku, Japan, [2]Department of Cardiovascular Control, Kochi Medical School, Nankoku, Japan, [3]Department of Pathology, Kochi Medical School, Nankoku, Japan and [4]Department of Urology, Kochi Medical School, Nankoku, Japan

Correspondence and offprint requests to: Yoshihiko Kakinuma; E-mail: kakinuma@kochi-u.ac.jp

Abstract

Background/aims. We have reported that tubular epithelial cell injury caused by renal ischemia–reperfusion is attenuated in conditional *VHL* knockout *(VHL-KO)* mice and also that induction of hypoxia-inducible factor (HIF) suppresses angiotensin II-accelerated Habu snake venom (HV) glomerulonephropathy in rats. However, it remains unknown whether *VHL* knockdown protects glomerular endothelial cells from endothelium-targeted glomerulonephritis.

Methods and results. *VHL-KO* mice with HV glomerulonephropathy (HV GN) had fewer injured glomeruli, a lower mesangiolysis score and reduced blood urea nitrogen levels. Immunoreactivity of vascular endothelial growth factor (VEGF) in the glomerular capillaries was enhanced by *VHL* knockdown and was conserved even in *VHL-KO* mice with HV GN, despite HV-attenuating endothelial VEGF expression *in vitro*. *VHL-KO* mice showed enhanced nitric oxide (NO) production in glomerular endothelial cells and tubular cells, associated with activated VEGF expression in the kidney (i.e. an activated NO–VEGF axis). The levels of NO in glomeruli and tubules were conserved even in mice with HV GN. In contrast, suppressing NO production in glomerular endothelial cells by an NO synthase inhibitor,

N_{ω}-nitro-L-arginase, completely blunted the protection of *VHL-KO* from HV GN. The activated NO-VEGF axis in the kidney of *VHL-KO* mice was also associated with an elevation in Flk-1 phosphorylation and increased levels of IL-10 and IP-10.

Conclusion. Conditional *VHL* knockdown may enhance the NO–VEGF axis and protect glomerular endothelial cells from HV GN, thereby providing resistance to injury of tubular epithelial cells and glomerular endothelial cells.

Keywords: Habu snake venom glomerulonephropathy; nitric oxide; vascular endothelial growth factor

Introduction

Using a model of acute glomerulonephopathy induced by Habu snake venom (HV GN) (a glomerular endothelium-targeted model), we have demonstrated that angiotensin II accelerates the formation of HV GN and that the kidneys are protected from glomerular injury by upregulation of a hypoxia-inducible factor (HIF)/vascular endothelial cell growth factor (VEGF) signaling pathway induced by cobalt chloride. In contrast, elevated von Hippel–Lindau protein (pVHL) exacerbates glomerular injury [1, 2]. Furthermore, using the Cre-lox P system in conditional *VHL* knockout (*VHL-KO)* mice, we demonstrated that renal tubular injury induced by ischemia–reperfusion injury was attenuated by deletion of *VHL* gene [3].

It is already known that the HIF system, represented by HIF-1α and HIF-2α, has a major role in protecting cells against hypoxic insult and that the level of these proteins is regulated by pVHL [4]. In hypoxia, disturbed interaction of HIF and VHL elevates the level of HIF-1α and upregulates downstream gene expression, including VEGF.

To date, we have carried out detailed investigations in conditional *VHL-KO* mice on the protective mechanism against acute renal tubular injury mediated by HIF-1, VEGF and downstream genes [3]. However, it remains unclear whether HIF-1α protein induction protects glomeruli from endothelial cell-targeted injuries. In *VHL-KO* mice, factors which are specifically responsible for cell protection remain difficult to be differentiated, as many downstream genes are simultaneously and sequentially transactivated by HIF-1α.

VEGF is one candidate that has a protective effect on glomerular capillary endothelial cells. Recently, it has been proposed that uncoupling of the VEGF–eNOS axis may trigger renal damage by upregulating VEGF expression and decreasing nitric oxide (NO) production [5]. This hypothesis suggests that eNOS-derived NO usually acts as a negative modulator against the effects of VEGF (i.e. proliferation of endothelial cells). Therefore, a balanced VEGF–eNOS axis appears to be needed for cell protection. On the basis of this hypothesis, pathological cell proliferation may result when the axis becomes unbalanced.

In this study, we used *VHL-KO* mice treated with HV to investigate the role of *VHL* gene knockdown on glomerular endothelial cells, with particular emphasis on the VEGF–eNOS axis.

Materials and methods

Cell culture

Human umbilical vein endothelial cells (HUVECs) were cultured in EGM-2 culture medium (Cambrex, Walkersville, MD) complemented with the suggested reagents and then treated with Habu snake venom (HV, 100 μg/mL, Sigma-Aldrich, St. Louis, MO) for 8 h. After this treatment, each sample was processed for western blot analysis.

Generation of VHL-KO mice

Mice carrying the floxed *VHL* allele were generated by Ma *et al.* [6], using Cre/lox site-specific recombination technology. To generate *VHL-KO* mice with inactivation in multiple tissues in an inducible manner, we crossed $VHL^{f/f}$ mice with $VHL^{d/+}$ mice which carried the tamoxifen-inducible Cre recombinase transgene, driven by a human β-actin promoter ($VHL^{f/d}CreER^{TM}$). To obtain an adequate number of mice for experiments, each $VHL^{f/d}CreER^{TM}$ mouse with the genetic background of C57BL6/J was crossed further to generate both $VHL^{f/f}CreER^{TM}$ *(VHL-KO)* mice and $VHL^{f/d}CreER^{TM}$ mice. One week before the experiments, the mice were injected intraperitoneally (i.p.) with tamoxifen in corn oil (4 mg/mouse) to activate Cre recombinase. For these experiments, 12–16-week-old male $VHL^{f/f}CreER^{TM}$ *(VHL-KO)* mice ($n = 11$), $VHL^{f/+}CreER^{TM}$ (*control*) mice ($n = 11$), heterogeneously VHL gene-deleted mice (*hetero VHL-KO*, i.e. $VHL^{del/+}$, $n = 3$) and *wild-type* mice (*wild-type*, $n = 3$) were administered tamoxifen to evaluate VEGF expression. The mice were housed in a specific pathogen-free facility, with routine serum analysis confirming they were negative for common murine viral pathogens.

Western blot analysis

Protein extracts from whole murine kidneys were prepared using Tissue Protein Extraction Reagent (Pierce Biotechnology, Rockfold, IL). Western blot analysis was performed as described in our previous study [7]. The protein extracts were mixed with sample buffer and the concentration of each sample was quantified precisely so that a comparable amount of protein was applied to each lane. The samples were separated by electrophoresis on sodium dodecyl sulfate–polyacrylamide gel electrophoresis gels and then transferred to polyvinylidene difluoride membranes (Immnbilion-P; Millipore, Bedford, MA). A rabbit polyclonal antibody against VHL (BD Bioscience), diluted at 1:500, and a polyclonal antibody against VEGF (Santa Cruz Biotechnology, Inc., Santa Cruz, CA), diluted at 1:200, were used in conjunction with a horseradish peroxidase-conjugated secondary antibody. The other primary antibodies used were against IL-10 (Abcam Inc., Cambridge, MA) diluted at 1:500; IP-10 (Abcam) diluted at 1:200; eNOS (Cell Signaling Technology, Danvers, MA) diluted at 1:200; phospho eNOS (Ser1177) (Cell Signaling Technology) diluted at 1:300 and phospho Flk-1 (Santa Cruz Biotechnology) diluted at 1:500. Comparability of sample loading volumes was confirmed by expression of α-tubulin and Coomassie brilliant blue staining.

A mouse model for Habu snake venom glomerulonephropathy

One week after *VHL-KO* mice had undergone unilateral nephrectomy, they were administered an intravenous injection of venom toxin *Trimeresurus flavoviridis* (6.5 mg/kg body weight, Sigma-Aldrich Chemicals) to induce Habu snake venom glomerulonephropathy (HV GN). This procedure was carried out according to modified protocols [1, 8]. One day after administration of HV, the mice were sacrificed for sampling, with some mice being processed by perfusion fixation. All the animals were housed in cages at a constant room temperature and humidity under a controlled light–dark cycle. The animals were fed with a standard diet. All the animal experiments were performed in accordance with the Japan Animal Protection Laws.

Tissue preparation

After the weight of the kidneys was measured, they were sliced transversely into 1-mm thick segments. Tissue sampling for morphometric analysis was performed using the area-weighted sampling technique, as described previously [9]. Paraffin sections that were 1–5 μm in thickness (five blocks per animal) were prepared for further study.

Semiquantitative analysis of mesangiolytic glomerular damage

A hallmark of HV GN is focal mesangiolysis, which is characterized by dissolution or disappearance of the mesangial matrix due to necrosis and

apoptosis of mesangial cells. In the glomeruli, mesangiolysis is associated with a loss of mesangial cells and capillary aneurysms. To analyze the extent of mesangiolysis, a semiquantitative mesangiolysis score was calculated in the periodic acid-Schiff stain (PAS)-stained paraffin sections. A total of 100 glomeruli were examined in each animal using the following scoring system: 0 no capillary changes; 1 capillary dilatation comprising <25% of the capillary convolute; 2 capillary dilatation comprising >25% of the capillary convolute or capillary aneurysm comprising <50% of the capillary convolute; 3 capillary aneurysm comprising 50–75% of the capillary convolute; 4 capillary aneurysm comprising >75% of the capillary convolute [9].

In *control* mice with HV GN, the mesangiolysis score was evaluated further by counting 20 glomeruli in both the medulla and cortex area. The difference between the scores was then analyzed.

Assessment of renal function

Blood urea nitrogen (BUN) and creatinine (Cr) levels were measured to assess renal function. BUN and Cr levels were analyzed by automated analysis (Hitachi 7350; Hitachi, Ibaragi, Japan) at our laboratory center. BUN and Cr levels were also measured in untreated *control* ($n = 6$) and *VHL-KO* mice ($n = 6$).

Immunohistochemical analysis

An immunohistochemical study was performed using the Ventana automated immunohistochemistry system (Discovery TM; Ventana Medical Systems, Inc., Tucson, AZ). VHL was identified by a polyclonal anti-VHL antibody, sc-5575 (1:150, BD Bioscience), VEGF by a monoclonal anti-VEGF antibody, sc-152 (1:100; Santa Cruz), CD31 by a monoclonal anti-CD31 antibody, M0823 (1:500; Dako, Hamburg, Germany) and von Willbrand Factor (vWF) by a polyclonal vWF antibody, A082 (1:500, Dako). Antigen retrieval was performed for 60 min using microwave treatment in a preheated Dako Target Retrieval Solution (pH 6.0; Dako, Glostrup, Denmark). This was followed by other steps that included inhibition of intrinsic peroxidase and blocking and reaction with a primary antibody.

In situ NO detection

Mice from each group were perfused through the left ventricle with prewarmed phosphate-buffered saline (PBS) at 37°C at a flow rate of 1 mL/min. This was followed by resection of the right atrium. After complete removal of their blood, the animals were perfused again at a flow rate of 1 mL/min for an additional 10 min with PBS that contained 0.01 mmol/L of diaminofluorescein-2 (DAF-2; Sekisui Medical, Tokyo, Japan) and 0.01 mmol/L of L-Arginine. After perfusion, the unreacted DAF-2 was removed by washing with PBS for 10 min. The NO fluorescent images of the 1-mm-thick renal tissue samples were examined using a fluorescence microscopy (Zeiss) with excitation at 490 nm and emission at 530 nm [10].

Assessment of NO involvement in protecting the kidney of VHL-KO mice from HV GN using an NOS inhibitor and an NO donor

In order to assess the involvement of NO in attenuating HV GN, we injected *VHL-KO* mice ($n = 5$) with a single bolus (12 mg/kg, i.p.) of the NOS inhibitor, N_{ω}-nitro-L-arginase (L-NNA), to 30 min prior to HV administration and then measured levels of BUN and Cr as well as mesangiolysis scores [11]. We also injected an NO donor, S-nitroso-*N*-acetyl-penicillamine (SNAP), (20 mg/kg, i.p.), 30 min before administration of HV ($n = 4$), followed by evaluation of renal function [12].

Statistical analysis

The data are expressed as the means ± SEM. The Mann–Whitney test was used to compare the two groups. In the case of multiple comparisons, differences among data were assessed by the Kruskal–Wallis test, followed by Scheffe's post hoc test. P-values <0.05 were considered statistically significant.

Results

The effects of Habu snake venom on expression of VEGF and VHL

Habu snake venom (HV) induces glomerulonephropathy (HV GN). In order to assess whether endothelial cells are targeted by HV, the expression levels of the proteins, VEGF and VHL were studied in HUVECs with and without the addition of HV (Figure 1). Initially, the VHL expression level increased >4 h period. In contrast, HV caused a gradual attenuation of VEGF expression within 8 h. However, the intact appearance of the cells suggested that HV targets endothelial cells to suppress the expression of VEGF, an endothelial cell-specific cell protective factor. Given that a comparable amount of protein was loaded in each lane, these results suggest that HV interferes specifically with endothelial VEGF expression.

Attenuation of Habu snake venom induced glomerulonephropathy in VHL-KO mice

To assess whether VHL inactivation plays a role in protecting glomerular endothelial cells in HV GN, the severity of the disease in *VHL-KO* (*VHL$^{f/f}$CreER^{TM}*) mice was compared with that in *control* (*VHL$^{f/+}$CreER^{TM}*) mice. Basal BUN levels in the HV-untreated *VHL-KO* (HV− in *VHL-KO*) (25.7 ± 1.1 mg/dL) and *control* mice (HV− in *control*) (25.2 ±1.5 mg/dL) were similar. Basal Cr levels were also not significantly different in *VHL-KO* mice (HV−) (0.25 ± 0.02 mg/dL) and *control* mice (HV−) (0.20 ± 0.03 mg/dL) (Figure 2A).

In *control* mice, HV administration (HV+ in *control*) caused a significant increase in BUN levels (60.8 ± 13.1 mg/dL) compared to nontreatment ($P < 0.05$ versus HV− in *control*) (Figure 2A). However, BUN levels in *VHL-KO* mice treated with HV (HV+ in *VHL-KO*) ($n = 11$) were significantly lower (28.4 ± 2.1 mg/dL), compared to HV-treated *control* mice ($P < 0.05$ versus HV+ in *control*)

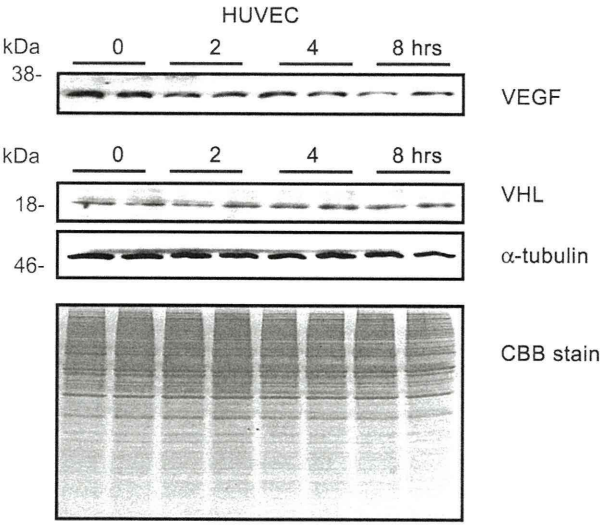

Fig. 1. Western blot analysis of VHL and VEGF expression in HUVECs with Habu snake venom. After the administration of 100 μg/mL of Habu snake venom (HV), the VHL protein expression level increases for 4 h and then stabilizes. However, HV causes a reciprocal decrease in VEGF expression level within 8 h. The application of comparable sample volumes is confirmed by Coomassie brilliant blue staining and the α-tubulin levels.

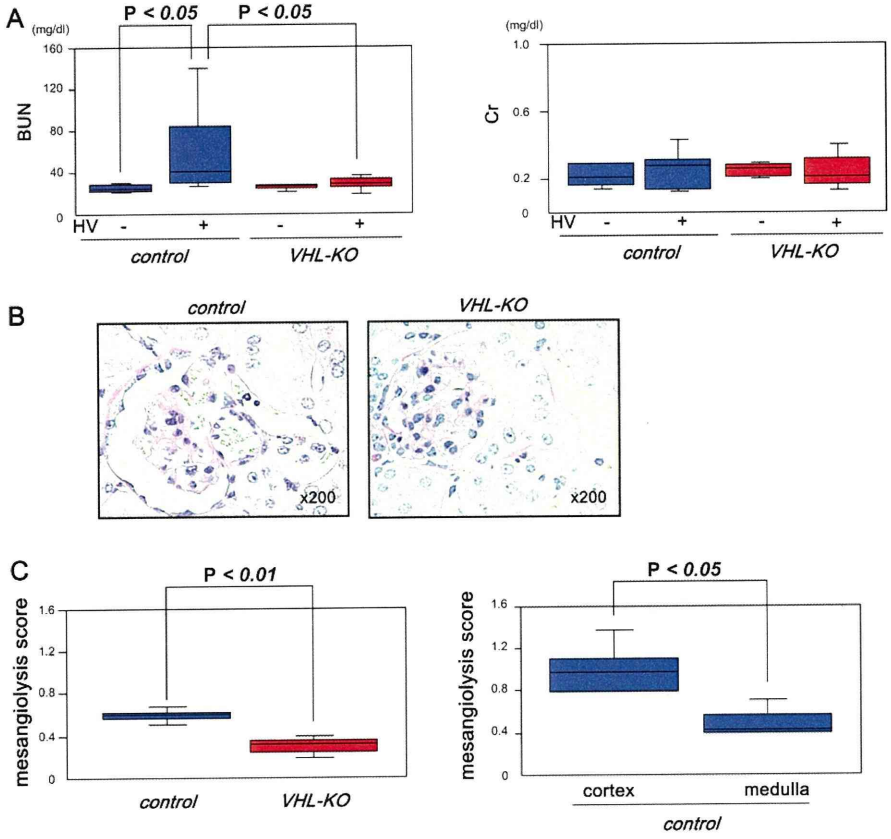

Fig. 2. Functional and pathological attenuation of Habu snake venom-induced glomerulonephropathy (HV GN) in *VHL-KO* mice. In *control* mice, HV (HV+ in *control*) causes significant increase in BUN levels compared with untreated mice ($P < 0.05$ versus HV−in *control*). In contrast, in *VHL-KO* mice with HV GN (HV+ in *VHL-KO*), BUN levels are significantly reduced, compared with *control* mice ($P < 0.05$ versus HV+ in *control*). There is no significant change in Cr levels (**A**). Glomerular damage from mesangiolysis is more evident in *control* mice (PAS stain, ×200) (**B**) with a mesangiolysis score of 0.60 ± 0.04 (**C**). In contrast, the severity of damage is significantly attenuated in *VHL-KO* mice (B), with a score of 0.31 ± 0.02 ($P < 0.001$ versus *control*) (C). In *control* mice with HV GN, the mesangiolysis score in the renal cortex (1.01 ± 0.096) is greater than that measured in the medulla (0.49 ± 0.05) ($P < 0.05$) (C).

($n = 11$) (Figure 2A). However, there was no significant difference in Cr levels between *VHL-KO* mice (HV+) (0.24 ± 0.13 mg/dL) and *control* mice (HV+) (0.25 ± 0.03 mg/dL) (Figure 2A).

The pathological features of HV GN were focal mesangiolysis (i.e. loss of mesangial cells) and capillary aneurysms in the glomeruli (Figure 2B). As a result, the glomeruli in the HV-treated *control* mice had more severe mesangiolysis with a higher mesangiolysis score of 0.60 ± 0.04. In *control* mice, further analysis of mesangiolysis in the cortex and medulla showed that injury was more evident in the cortex (mesangiolysis score of 1.01 ± 0.10) than the medulla (0.49 ± 0.05) (Figure 2C). In contrast, the severity of injury was significantly attenuated in *VHL-KO* mice, with a mesangiolysis score of 0.31 ± 0.02 ($P < 0.001$ versus *control*) (Figure 2C). Neither *VHL-KO* mice nor *control* mice had pathological lesions in the renal tubules and had negligible numbers of infiltrated inflammation cells. This suggests that VHL inactivation contributes to the protection of glomerular endothelial cells from HV-induced capillary damage.

Increased VEGF expression in glomeruli of VHL-KO mice

One week after administration of tamoxifen, VHL protein expression was reduced in the kidneys of *VHL-KO* mice compared with that in *control* mice (Figures 3A). A decrease in VHL immunoreactivity was observed, especially in the proximal tubules (Figure 3B). In contrast, VEGF expression was increased in glomeruli, especially glomerular endothelial cells, with the localization pattern of VEGF signals being comparable with that of CD31 and vWF in glomeruli from *VHL-KO* mice (Figure 3C).

In each genotype (*wild-type, hetero VHL-KO* and *control*) showing positive VEGF signals in glomeruli, with the exception of *VHL-KO*, the intensity of VEGF signals in glomeruli was remarkably reduced by HV. In contrast, VEGF signals were sustained in *VHL-KO* mice (*VHL-KO* in Figure 3D). In *VHL-KO* mice alone, VEGF immunoreactivity in glomerular capillaries was still evident with VEGF-positive signals being sustained clearly in the glomerular capillaries even following induction of HV GN. These findings were confirmed by western blot analysis (Figure 3E).

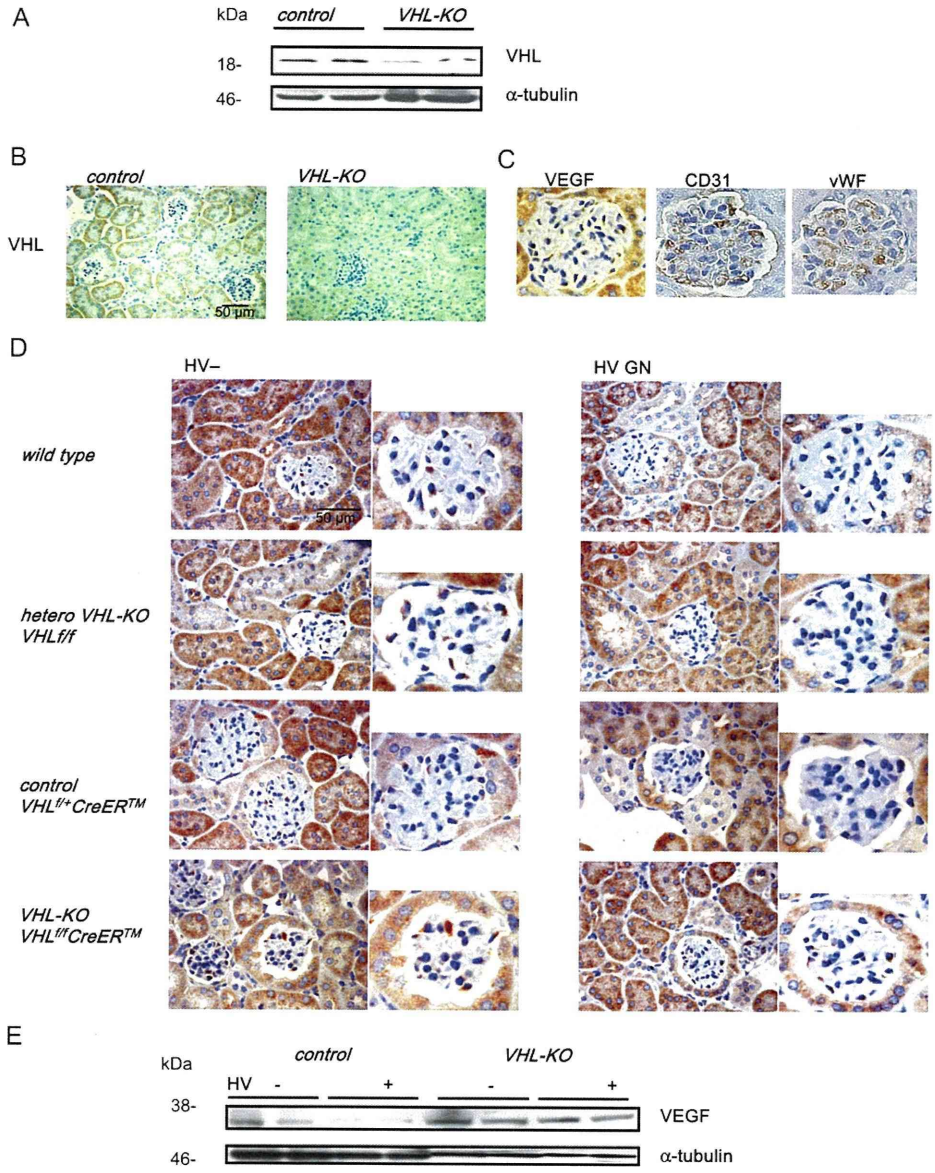

Fig. 3. VEGF is upregulated in glomerular endothelial cells in *VHL-KO* mice and VEGF signals are not attenuated in HV GN. Western blot analysis and immunohistochemical studies both demonstrate that pVHL, which is expressed predominantly in renal tubular cells, especially the proximal tubules, is decreased in *VHL-KO* mice. Two separate samples from each group are shown (**A**, **B**). The localization pattern of VEGF-positive cells is similar to that of CD31 and vWF, suggesting that VEGF is expressed in the endothelial cells (**C**). In comparison, the expression patterns of VEGF in *wild-type* mice (*wild-type*), heterogeneously VHL-deleted mice ($VHL^{del/+}$, *hetero VHL KO*) and *control* mice ($VHL^{f/+}CreER^{TM}$, *control*) show that VEGF-positive signals are localized in the glomeruli. In contrast, in *VHL-KO* mice (*VHL-KO*), strong VEGF signals are detected in glomerular endothelial cells (each genotype with HV−, left panel in **D**). Glomerular VEGF is still expressed in endothelial cells of *VHL-KO* mice even following induction of HV GN. However, in *control* mice with HV GN, as well as HV-treated *wild-type* and *hetero VHL-KO*, few VEGF signals in glomeruli are detected (HV GN, right panel in D). Western blot analysis reveals that VEGF expression in the kidneys of *VHL-KO* mice with HV GN is sustained and increased compared with the HV-treated *control* mice. Two separate samples representing each group are applied for the analysis (**E**).

Upregulation of a VEGF–NO pathway in VHL-KO mice

The VEGF–NO pathway was investigated to determine the mechanisms responsible for VHL deletion-mediated glomerular protection against HV GN in *VHL-KO* mice. As VEGF reportedly triggers NO production by eNOS, the renal NO production level in *control* and *VHL-KO* mice, both not treated with HV, was initially compared using the *in situ* NO indicator DAF-2 (Figure 4A). The signal level of NO was markedly upregulated in the glomeruli and renal tubules of the *VHL-KO* mice, compared with *control* mice. This suggests that the VEGF–NO pathway is activated by VHL deletion. Western blot analysis also demonstrated enhanced expression of phosphorylated eNOS and phosphorylated Flk-1 (VEGF type 2 receptor) in *VHL-KO* mice, but showed comparable levels of total eNOS in *VHL-KO* and *control* mice (Figure 4B).

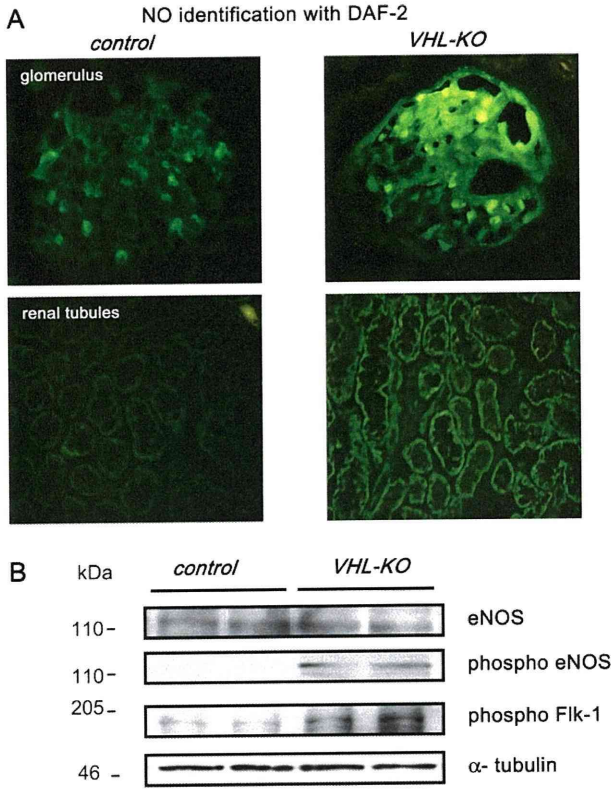

Fig 4. The increase in NO production in *VHL-KO* mice evaluated by DAF-2. In *VHL-KO* mice, the signal level of NO is upregulated markedly in the glomeruli and renal tubules compared with *control* mice. NO signals are clearly detected in endothelial cells in the glomeruli (**A**). Western blot analysis shows that phosphorylation of eNOS and Flk-1, a VEGF type 2 receptor, is upregulated in *VHL-KO* mice, with comparable levels of total eNOS being observed. Two separate samples in each group are shown (**B**).

Involvement of NO in protection of glomeruli from HV GN

HV completely eradicated NO-positive cells in the glomeruli and tubules in the *control* mice (*control*, Figure 5A). In contrast, in accordance with the effect of VHL deletion to attenuate glomerular injury, NO levels in the glomeruli of *VHL-KO* mice were also conserved in HV GN, with more NO-positive glomerular and renal tubular cells being observed (*VHL-KO* in Figure 5A). To further investigate the role of NO in protecting glomeruli from HV GN, we administered an NO donor, SNAP, to *control* mice suffering from HV GN and an NOS inhibitor, L-NNA, to *VHL-KO* mice with HV GN. The dose of each NO donor and NOS inhibitor was sufficient to modulate NO production in the kidney as assessed by DAF-2 perfusion. In *control* mice with HV GN, SNAP increased NO-positive glomeruli and renal tubules (*control* + SNAP), compared with HV GN alone (*control*). Furthermore, in *VHL-KO* mice with HV GN treated with L-NNA, the level of NO production was decreased markedly in both glomeruli and renal tubules (*VHL-KO* + L-NNA) compared with *VHL-KO* mice suffering from HV GN (*VHL-KO*).

Modulation of NO production with either an NO donor or an NOS inhibitor affected renal function in HV GN. In *control* mice with HV GN, SNAP-treated mice (SNAP+ in *control*) showed a trend toward reduced BUN and Cr levels (30.0 ± 3.2, 0.15 ± 0.01 mg/dL, respectively), although this reduction was not significantly different from that observed in non-SNAP-treated *control* mice (SNAP− in *control*) (Figure 5B). However, the mesangiolysis score of SNAP-treated *control* mice with HV GN (SNAP+ in *control*) was suppressed (0.40 ± 0.03, $P < 0.01$) compared with non-SNAP-treated mice (Figure 5C). On the other hand, L-NNA caused marked elevation in BUN and Cr levels in *VHL-KO* mice (L-NNA+ in *VHL-KO*) treated with HV compared with HV alone (L-NNA− in *VHL-KO*) (BUN 98.5 ± 16.8, Cr 0.69 ± 0.17, $P < 0.05$). As a result of the deterioration in renal function, the mesangiolysis score was markedly increased by L-NNA (1.03 ± 0.10, $P < 0.01$) (Figure 5C). These results indicate that one of the renoprotective mechanisms against HV-induced glomerular injury in *VHL-KO* mice is dependent on NO production.

Regulation of other factors enhanced in VHL-KO mice

To search for other factors that may be involved in protecting endothelial cells from glomerular injury, we investigated the protein expression levels of IL-10 and IP-10. The expression levels of IL-10 and IP-10 in *control* mice were decreased by HV, whereas the levels were sustained in *VHL-KO* mice even following HV administration (Figure 6).

Discussion

Our previous studies have revealed that coadministration of HV and angiotensin II accelerates aggravation of glomerulonephropathy in rats [1] and that upregulation of *VHL* enhances the progression of glomerulonephopathy [2]. This occurs despite *VHL* being a known substrate-docking interface that specifically recognizes prolyl-hydoroxylated HIF-1α for ubiquitin [13]. A recent study, which we carried out, also indicated that HIF-1α, HIF-2α and VEGF were upregulated in *VHL* conditional knockout (*VHL-KO*) mice, in which tamoxifen administration under normoxia initiated inactivation of pVHL, with renal tubular epithelial cells in the mice becoming resistant to ischemia–reperfusion injury [3]. This suggests that deletion of the *VHL* gene is responsible for protecting renal tubular cells. However, it remains to be established whether *VHL* gene deletion also plays a role in protecting glomerular endothelial cells from glomerulonephropathy. In this study, we induced HV GN in *VHL-KO* mice as a glomerular endothelial cell-targeted model. The mesangioproliferative nephropathy that develops in this condition represents a glomerulus-specific injury with mesangial proliferation and detachment of degenerative epithelial and endothelial cells.

Our *in vitro* studies demonstrated that expression of pVHL in endothelial cells was upregulated by HV. In contrast, VEGF expression was downregulated, indicating that the expression patterns of VHL and VEGF are reciprocally regulated and that HV targets endothelial cells and

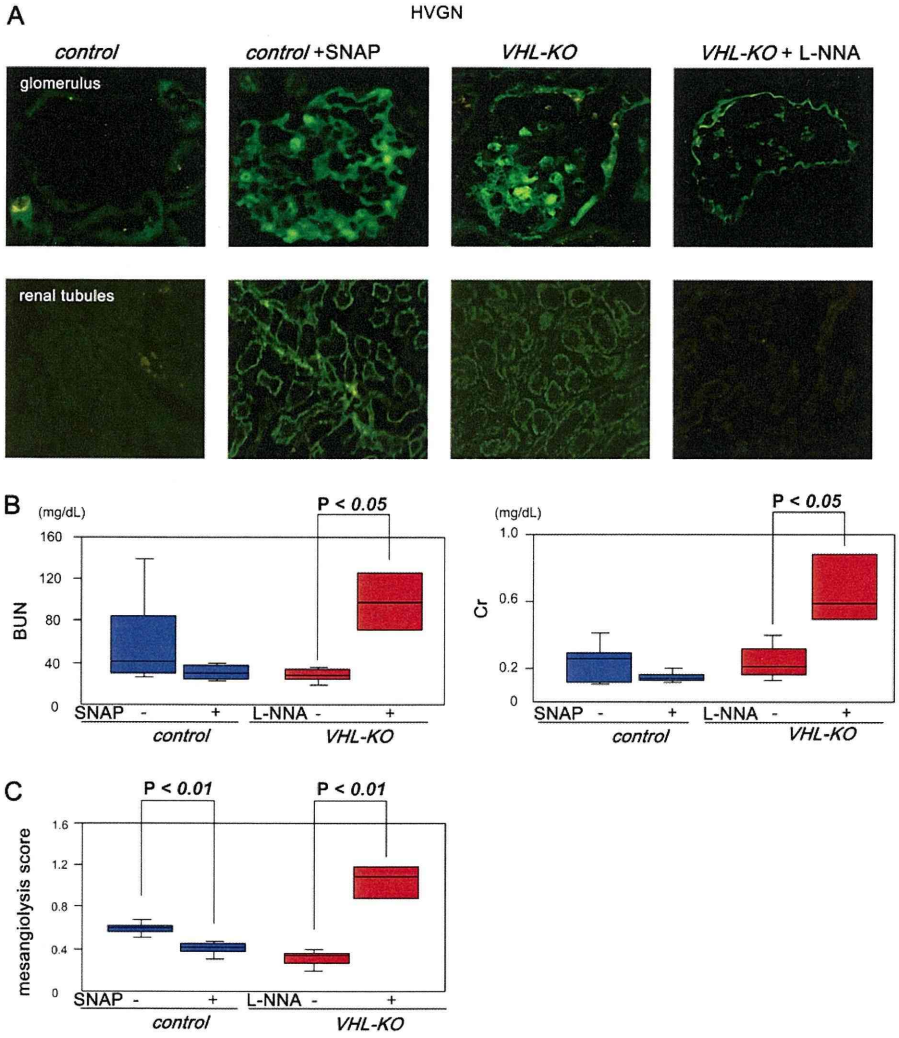

Fig. 5. The NO has a renoprotective role against HV GN in *VHL-KO* mice. In *control* mice with HV GN, NO signals are completely attenuated throughout the kidney, especially in the glomeruli (*control*). However, in *VHL-KO* mice with HV GN, NO signals are still detected in the glomeruli and renal tubules (*VHL-KO*). In *control* mice with HV GN treated with SNAP, NO signals are still detected in the glomeruli and renal tubules (+SNAP). In *VHL-KO* mice with HV GN treated with L-NNA, NO signals are completely reduced throughout the kidney, especially in the glomeruli (+L-NNA) (**A**). Comparison of *control* mice with HV GN (SNAP−) and SNAP-treated mice with HV GN (SNAP+) shows a trend of decreasing BUN and Cr levels and a significant reduction in mesangiolysis score by SNAP ($P < 0.01$) (**B**, **C**). On the other hand, the *VHL-KO* mice with HV GN treated with L-NNA (L-NNA+) shows impaired renal function with marked elevation in BUN and Cr ($P < 0.05$) and a higher mesangiolysis score ($P < 0.01$) (B, C).

modulates their gene expression. In our *in vivo* studies, *VHL-KO* mice subjected to HV showed less severe mesangiolysis than *control* mice, as demonstrated by lower mesangiolysis scores. This suggests that pVHL inactivation may ameliorate HV GN. Hass *et al.* [9] reported that HV induced a HV GN peak 1 day after injection of HV, with an average mesangiolysis score of 0.6. This score was comparable to those measured in *control* mice in our present study. Further analysis comparing the scores in the cortex and medulla revealed that the cortex was more severely injured in the control kidneys, with a greater reduction in VEGF signals in this area. As a result of HV GN, immunoreactivity for VHL was present predominantly in the renal cortex, especially in the proximal tubules. In contrast, VEGF signals, which became weaker in the cortex following induction of HV, were relatively restricted in the medulla. This finding is in agreement with our previous study that showed that pVHL is expressed exclusively in the proximal tubules. Renal function indices also confirmed the pathological differences in HV GN between *VHL-KO* and *control* mice. BUN levels were significantly decreased in *VHL-KO* mice, compared with *control* mice, while Cr levels tended to be lower, despite basal levels of BUN and Cr in two groups of mice being similar. A BUN level is rapidly affected by a kidney injury, specifically from mesangiolysis, therefore the alteration of BUN appears in the early phase of renal injury. In contrast, the level of Cr is dependent on GFR, and HV GN, unlike acute tubular necrosis, does not affect GFR in the acute phase. This might be a reason for the discrepancy.

Our *VHL-KO* mice characteristically showed enhanced VEGF expression in renal tubular cells and glomerular endothelial cells. As previously reported [14], HV causes marked suppression of VEGF expression in the glomeruli.

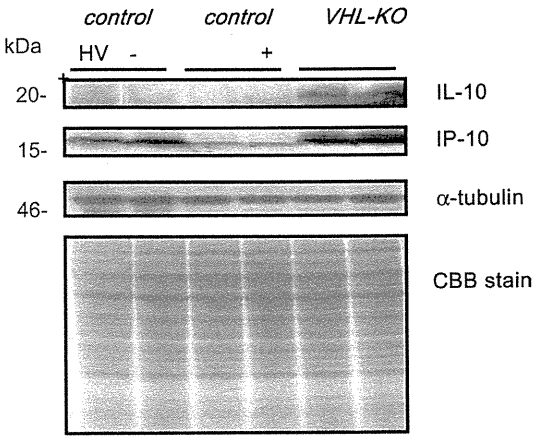

Fig. 6. Western blot analysis of IL-10 and IP-10 in the kidneys of *VHL-KO* mice. The protein expression levels of IL-10 and IP-10 are sustained in *VHL-KO* mice (HV+), compared with the *control* mice (HV+ in *control*). However, HV attenuates IL-10 and IP-10 expression in the kidney. Two separate samples in each group are shown.

Hypoxia and other stressors reportedly upregulate VEGF expression in the glomerulus [14, 15]. In several models of experimental glomerulonephropathy induced by either anti-Thy-1.1 antibody or HV, the systemic administration of VEGF also reportedly accelerates the repair of injured glomerular capillaries and prevents glomerular sclerosis [16]. Furthermore, the renoprotective effects of estrogen, which preserve the function of microvascular endothelium, are also partially mediated by VEGF [17]. It has also been reported that reduced VEGF expression is accompanied by progressive loss of glomerular and peritubular capillaries, resulting in the development of glomerulosclerosis and tubulointerstitial fibrosis, respectively [18]. Taken together, this evidence suggests that VEGF plays a major role in protecting the kidney from glomerulonephropathy.

However, upregulation of VEGF in response to renal injury does not always lead to a favorable outcome, especially in the case of VEGF treatment of the kidneys with dysfunctional endothelial cells [19]. In diabetes, VEGF is known to cause glomerular and tubular hypertrophy associated with increased urinary albumin excretion and glomerular hyperfiltration [20]. Angiotensin II also increases plasma VEGF levels and activates the local VEGF system by causing systemic hypertension and tubulointerstitial injury [21, 22]. Despite such unexpected side effects of VEGF, it has also been reported that VEGF activates NO production by increasing eNOS expression and that this balanced activation of the VEGF–NO pathway induces a survival signal in endothelial cells that sustains the function [23]. In ischemic conditions, NO contributes to protection of the kidney, whereas NO inhibitors accelerate ischemic renal injury [12, 24]. These findings indicate that as long as endothelial cell function remains intact with adequate levels of NO being produced, as demonstrated in *VHL-KO* mice, VEGF will exert balanced dual effects, including a cell-proliferative, cell-protective and NO-producing effects.

The DAF-2 perfusion and staining experiments in the present study demonstrated that NO production is increased in *VHL-KO* mice. In these mice, the intensity of NO signals was enhanced in the renal tubules and in the glomeruli, especially in endothelial cells. This suggests that NO production is increased in both types of cells. This model is therefore characterized by balanced enhancement of NO and VEGF production. As demonstrated in our study, the eNOS and VEGF type 2 receptors in *VHL-KO* mice were phosphorylated more efficiently than in *control* mice (Figure 4), a finding that supports our hypothesis.

To investigate whether NO was a crucial factor protecting glomerular cells in *VHL-KO* mice, an NO donor, SNAP, was administered to HV-treated *control* mice, and an NOS inhibitor, L-NNA, administered to HV-treated *VHL-KO* mice. Production of NO that is reduced by HV was sustained by SNAP in *control* mice even following administration with HV. On the other hand, in *VHL-KO* mice with elevated NO levels, administration of L-NNA completely blunted NO production in glomerular endothelial cells and renal tubular cells. In agreement with our findings on NO production in *control* mice, administration of SNAP was also associated with a trend of reduced BUN and Cr levels and a significant decrease in mesangiolysis score. In contrast, L-NNA suppressed NO production in *VHL-KO* mice with higher NO levels, resulting in aggravation of renal function and tissue damage.

On the basis of these findings, we consider the advantages of dual enhancement of NO production and VEGF expression in this model are as follows. As evidenced in previous reports [25–29], NO plays an anti-inflammatory role by inhibiting leukocyte migration and adhesion of platelets and monocytes to the microvascular endothelium. There is also evidence that NO protects endothelial cells from apoptosis induced by high glucose exposure and attenuates renal damage in ischemia–reperfusion injury [30]. As already mentioned, enhanced VEGF expression appears to play a pivotal role in pathological angiogenesis. However, unlike previous reports [6], our *VHL-KO* mice did not develop any capillary-rich tumors, other than hemangiomas, after *VHL* gene deletion during their lifetime.

The expression of IL-10 and IP-10, which are both known renal protective factors, was increased in the kidneys of *VHL-KO* mice. The fact that T lymphocytes produce IL-10, an immunosuppressive cytokine, led us to focus on its role as an inhibitor of tumor angiogenesis [31, 32]. IL-10 is also a potent anti-inflammatory cytokine that works partly by upregulating endothelial NO synthase [33, 34]. Although the cellular source of IL-10 was not completely investigated in the current study, our findings suggest the mechanism that attenuates HV glomerulonephropathy in *VHL-KO* mice is partly mediated by NO production via VEGF and/or IL-10. Furthermore, IP-10, which is also upregulated in *VHL-KO* mice, reportedly competes against the effects of VEGF and negatively modulates angiogenesis, resulting in the death of cells in newly formed blood vessels. This suggests that IP-10 may regulate against excessive angiogenesis [35]. The mechanism responsible for upregulating IP-10 expression may therefore be a response to the overexpression of VEGF and may counteract the actions of VEGF, which is markedly expressed in *VHL-KO* mice. IP-10 also reportedly possesses an inhibitory effect on tubular cell proliferation *in vivo* and

in vitro [36]. Consequently, upregulation of IP-10 may protect glomerular and interstitial tissue in the kidney from HV.

The side effects of chronic *VHL* knockdown were never observed pathologically or morphologically in the kidney and other organs in our *VHL-KO* mice. Further study is therefore needed to investigate the chronic phenotypes of *VHL* gene deletion.

In conclusion, this study indicates that VHL deletion activates the NO–VEGF axis properly to salvage glomerular endothelial cells from glomerulonephropathy.

Acknowledgements. This research was supported by Grants-in-Aid from the Japan Society for the Promotion of Science (19590251, 21590283).

Conflict of interest statement. None declared.

References

1. Kudo Y, Kakinuma Y, Mori Y *et al.* Hypoxia-inducible factor-1alpha is involved in the attenuation of experimentally induced rat glomerulonephritis. *Nephron Exp Nephrol* 2005; 100: e95–e103
2. Kudo Y, Kakinuma Y, Iguchi M *et al.* Modification in the von Hippel-Lindau protein is involved in the progression of experimentally induced rat glomerulonephritis. *Nephron Exp Nephrol* 2007; 106: e97–e106
3. Iguchi M, Kakinuma Y, Kurabayashi A *et al.* Acute inactivation of the VHL gene contributes to protective effects of ischemic preconditioning in the mouse kidney. *Nephron Exp Nephrol* 2008; 110: e82–e90
4. Richard D, Berra E, Pouyssegur J. Nonhypoxic pathway mediates the induction of hypoxia-inducible factor-1alpha in vascular smooth muscle cells. *J Biol Chem* 2000; 275: 26765–26771
5. Nakagawa T. Uncoupling of the VEGF-endothelial nitric oxide axis in diabetic nephropathy: an explanation for the paradoxical effects of VEGF in renal disease. *Am J Physiol Renal Physiol* 2007; 292: F1665–F1672
6. Ma W, Tessarollo L, Hong S *et al.* Hepatic vascular tumors, angiectasis in multiple organs, and impaired spermatogenesis in mice with conditional inactivation of the VHL gene. *Cancer Res* 2003; 63: 5320–5328
7. Kakinuma Y, Ando M, Kuwabara M *et al.* Acetylcholine from vagal stimulation protects cardiomyocytes against ischemia and hypoxia involving additive non-hypoxic induction of HIF-1alpha. *FEBS Lett* 2005; 579: 2111–2118
8. Cattell V, Bradfield J. Focal mesangial proliferative glomerulonephritis in the rat caused by habu snake venom. A morphologic study. *Am J Pathol* 1977; 87: 511–524
9. Haas C, Câmpean V, Kuhlmann A *et al.* Analysis of glomerular VEGF mRNA and protein expression in murine mesangioproliferative glomerulonephritis. *Virchows Arch* 2007; 450: 81–92
10. Kuwabara M, Kakinuma Y, Ando M *et al.* Nitric oxide stimulates vascular endothelial growth factor production in cardiomyocytes involved in angiogenesis. *J Physiol Sci* 2006; 56: 95–101
11. Park KM, Byun JY, Kramers C *et al.* Inducible nitric-oxide synthase is an important contributor to prolonged protective effects of ischemic preconditioning in the mouse kidney. *J Biol Chem* 2003; 278: 27256–27266
12. Shin IC, Kim HC, Swanson J *et al.* Anxiolytic effects of acute morphine can be modulated by nitric oxide systems. *Pharmacology* 2003; 68: 183–189
13. Maynard MA, Ohh M. von Hippel-Lindau tumor suppressor protein and hypoxia-inducible factor in kidney cancer. *Am J Nephrol* 2004; 24: 1–13
14. Abe-Yoshio Y, Abe K, Miyazaki M *et al.* Involvement of bone marrow-derived endothelial progenitor cells in glomerular capillary repair in habu snake venom-induced glomerulonephritis. *Virchows Arch* 2008; 453: 97–106
15. Iruela-Arispe L, Gordon K, Hugo C *et al.* Participation of glomerular endothelial cells in the capillary repair of glomerulonephritis. *Am J Pathol* 1995; 147: 1715–1727
16. Kelly D, Hepper C, Wu L *et al.* Vascular endothelial growth factor expression and glomerular endothelial cell loss in the remnant kidney model. *Nephrol Dial Transplant* 2003; 18: 1286–1292
17. Kang D, Yu E, Yoon K *et al.* The impact of gender on progression of renal disease: potential role of estrogen-mediated vascular endothelial growth factor regulation and vascular protection. *Am J Pathol* 2004; 164: 679–688
18. Kang D, Hughes J, Mazzali M *et al.* Impaired angiogenesis in the remnant kidney model: II. Vascular endothelial growth factor administration reduces renal fibrosis and stabilizes renal function. *J Am Soc Nephrol* 2001; 12: 1448–1457
19. Cooper M, Vranes D, Youssef S *et al.* Increased renal expression of vascular endothelial growth factor (VEGF) and its receptor VEGFR-2 in experimental diabetes. *Diabetes* 1999; 48: 2229–2239
20. de Vriese A, Tilton R, Elger M *et al.* Antibodies against vascular endothelial growth factor improve early renal dysfunction in experimental diabetes. *J Am Soc Nephrol* 2001; 12: 993–1000
21. Masuda Y, Shimizu A, Mori T *et al.* Vascular endothelial growth factor enhances glomerular capillary repair and accelerates resolution of experimentally induced glomerulonephritis. *Am J Pathol* 2001; 159: 599–608
22. Zhao Q, Egashira K, Inoue S *et al.* Vascular endothelial growth factor is necessary in the development of arteriosclerosis by recruiting/activating monocytes in a rat model of long-term inhibition of nitric oxide synthesis. *Circulation* 2002; 105: 1110–1115
23. Ziche M, Morbidelli L, Choudhuri R *et al.* Nitric oxide synthase lies downstream from vascular endothelial growth factor-induced but not basic fibroblast growth factor-induced angiogenesis. *J Clin Invest* 1997; 99: 2625–2634
24. Chander V, Chopra K. Protective effect of nitric oxide pathway in resveratrol renal ischemia-reperfusion injury in rats. *Arch Med Res* 2006; 36: 19–26
25. Ialenti A, Ianaro A, Maffa P *et al.* Nitric oxide inhibits leukocyte migration in carrageenin-induced rat pleurisy. *Inflamm Res* 2000; 49: 411–427
26. Cuzzocrea S, Chatterjee PK, Mazzon E *et al.* Role of induced nitric oxide in the initiation of the inflammatory response after postischemic injury. *Shock* 2002; 18: 169–176
27. Ho FM, Liu SH, Liau CS *et al.* Nitric oxide prevents apoptosis of human endothelial cells from high glucose exposure during early stage. *J Cell Biochem* 1999; 75: 258–263
28. Kim HW, Greenburg AG. Nitric oxide scavenging, alone or with nitric oxide synthesis inhibition, modulates vascular hyporeactivity in rats with intraperitoneal sepsis. *Shock* 2002; 17: 423–426
29. Radomski MW, Palmer RMJ, Moncada S. Endogenous nitric oxide inhibits human platelet adhesion to vascular endothelium. *Lancet* 1987; 2: 1057–1058
30. Milsom A, Patel N, Mazzon E *et al.* Role for endothelial nitric oxide synthase in nitrite-induced protection against renal ischemia-reperfusion injury in mice. *Nitric Oxide* 2010; 22: 141–148
31. Kohno T, Mizukami H, Suzuki M *et al.* Interleukin-10-mediated inhibition of angiogenesis and tumor growth in mice bearing VEGF-producing ovarian cancer. *Cancer Res* 2003; 63: 5091–5094
32. Elenkov I, Chrousos G. Stress hormones, proinflammatory and anti-inflammatory cytokines, and autoimmunity. *Ann N Y Acad Sci* 2002; 966: 290–303
33. Cattaruzza M, Słodowski W, Stojakovic M *et al.* Interleukin-10 induction of nitric-oxide synthase expression attenuates cd40-mediated interleukin-12 synthesis in human endothelial cells. *J Biol Chem* 2003; 278: 37874–37880
34. Silvestre J, Mallat Z, Duriez M *et al.* Antiangiogenic effect of interleukin-10 in ischemia-induced angiogenesis in mice hindlimb. *Circ Res* 2000; 87: 448–452
35. Furuichi K, Wada T, Kitajima S *et al.* IFN-inducible protein 10 (CXCL10) regulates tubular cell proliferation in renal ischemia-reperfusion injury. *Nephron Exp Nephrol* 2008; 109: c29–c38
36. Bodnar R, Yates C, Rodgers M *et al.* IP-10 induces dissociation of newly formed blood vessels. *J Cell Sci* 2009; 122: 2064–2077

Received for publication: 22.7.10; Accepted in revised form: 10.3.11

In the Spotlight: BioInstrumentation

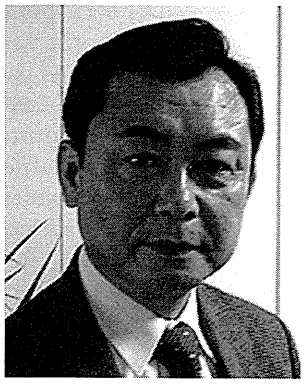

Ken-ichi Yamakoshi, *Member, IEEE*

OVER the major part of the last century medical instruments based on a variety of principles and technologies were developed for the measurement of physiological variables to aid diagnosis and medical treatment in the hospital as well as in the out-patient clinic. More latterly, however, there has been a growing interest and effort to obtain vital signs during normal daily life to achieve healthcare management at home. In order to realize this goal, it appears necessary to develop automatic means for the acquisition of the required physiological data and to implement this in a noninvasive fashion. It might also be of value to people in their home during daily routines to assist them by monitoring the usage of the home services and facilities in a fully automated manner.

The concept of this human support system, including features aimed at achieving home healthcare, is generally referred to as a "smart home" or "smart house." This has several elements, in particular: 1) as far as possible measurements should be made automatically, with only minimal operation required by the subjects; 2) monitoring should be continuous and around the clock; 3) the intended subjects might be elderly, physically or mentally challenged, at risk of illness, but not necessarily having an existing medical condition.

The development of the smart home through modern technological advances has progressed remarkably, and the present "In the Spotlight" column focuses on the various topics within this research area and briefly introduces several trials where recent advances have been made.

I. Progress in the Emergence of the Smart Home

The "smart home" or "smart house" is an intelligent residential environment to subserve inhabitants' needs and has been considered to be one of the most desirable dwellings of the future [1]. The first clear description of the smart home concept appears to have been presented by M. Weiser in 1991 [2]. The vision was of a place where many computers and electronic devices with wire/wireless communications were installed to support living environments. This work has also been well recognized as possibly the first proposal of "ubiquitous computing" or "pervasive computing." The author's concept is neatly encapsulated in the subtitle of the report, as *"Specialized elements of hardware and software, connected by wires, radio waves and infrared, will be so ubiquitous that no one will notice their presence."* This proposal included almost all of the constituent elements of the current smart home trials (and also ubiquitous computing), with the exception of the specific provision of healthcare services. After this key published work, many proposals have been made to create smart homes with modern technologies.

Currently, an important aspect of smart homes under discussion and being developed is the inclusion of healthcare services. Of relevance here is the activity of CENELEC (European Committee for Electro-technical Standardization), which has produced a roadmap for an integrated set of standards for the "smart home [3]." This roadmap includes several applications of services such as broadband communication, multimedia and entertainment, safety and security, home automation, energy management, and, significantly, telecare and healthcare. With regard to the implementation of smart home designs the recent and on-going advances within information communication technology (ICT) and pervasive computing have yielded new devices with appropriate characteristics [1]: 1) miniature—devices can be blended with or disappear into the environment; 2) communication—devices can communicate with other equipment; 3) autonomy—devices can work autonomously. These characteristics are also ideal for use in smart home healthcare systems, and this review will therefore focus on current technologies of the smart home incorporating healthcare services.

II. Smart Home for Healthcare

The concept of healthcare within smart homes often arises from a recognition of the growing importance of the so-called aging society within the community, countries or, indeed, the

Manuscript received September 21, 2011; accepted October 11, 2011. Date of publication October 19, 2011; date of current version January 06, 2012.

K. Yamakoshi is with the College of Science & Engineering and the Graduate School of Natural Science & Technology, Kanazawa University, Kakuma, Kanazawa 920-1192, Japan (e-mail: yamakosi@t.kanazawa-u.ac.jp).

Digital Object Identifier 10.1109/RBME.2011.2172599

whole world. A smart home equipped with sensors, actuators, and biomedical instruments may provide a better and more cost-effective living environment for elderly care in a person's own home. This could be achieved in an unrestrained manner, offering better independence, helping to maintain a good health condition as well as preventing social isolation. This system would also have networking means for communication between devices in the home and with a remote center and/or a family living remotely. Chan *et al.* gave a good review of this concept, introducing 13 smart home projects in the USA, the U.K. and Japan [4]. In addition, it is pertinent that these authors discussed in detail both advantages and disadvantages of the approach. The disadvantages identified by them are as follows: The smart home 1) involves a technology-push type rather than a demand-pull approach; 2) lacks interchangeability between a healthcare professional person and the system; 3) has difficulties of acceptance due to social, ethical and legal barriers; 4) requires considerable time and cost to operate the system; 5) can have privacy problems. It is also pointed out that it is doubtful if the present smart home technologies can truly lead to reduced healthcare costs in the future [5]. Although the above issues are open to debate, further evaluation of these possible disadvantages should be carried out carefully because of the impact on what is a seminal issue with implications for the practical realization of smart homes in the near future.

III. Bioinstrumentation for the Smart Home

Biomedical instrumentation constitutes an important, indeed essential element of the smart home [1], [3], [4], as reviewed recently by Ding *et al.* [6]. These authors categorized sensor technologies for the smart home into five types: 1) simple binary sensors (SBSs), 2) video cameras (VCs), 3) radio frequency identification devices (RFID), 4) infrastructure mediated systems (IMSs), and 5) other sensors. Motion detectors, pressure sensors, and contact switches are used as SBSs, indicating the presence of a human or their movement with a single digit "1" or "0." IMSs utilize motion sensors to determine human behavior in the house, these being positioned in such infrastructures as central heating, ventilation, air conditioning and so on. Other sensors used include environmental sensors to detect humidity, temperature, light and barometric pressure, and a microphone or a pneumatic strip installed under the bed linen to detect presence, respiration, cardiac pulse and body movements in the bed.

Skubic *et al.* have reported their efforts to develop smart home-based bioinstrumentation [7]. They investigated the construction of sensor-network systems for monitoring the behavior of elderly people in their own homes situated within the TigerPlace, an aging-in-place community located in Columbia, MO, USA [8]. The authors equipped and installed their network systems in 17 apartments and reported the operational monitoring status, which lasted in some cases more than two years [7]. The sensors used in this work were quite standard motion sensors, video sensors, and a bed sensor capable of capturing restlessness in sleep, cardiac pulse and respiration rates. The bed sensor consisted of a hydraulic sensor placed beneath a standard mattress [9].

An appropriate combination of signals obtained from several SBSs is able to give quite effective information about human behavior at home [4], [10], [11]. In general, however, it is difficult to perform a detailed analysis of human behavior due to the lack of standardization or generalization of the analysis methodology, and the use of different sensor positioning in the home, as well as the performance specification of sensors to be used. Recently, Hong *et al.* tried to overcome these problems [12]. They described a general ontology network of human activity using sensors positioned appropriately, giving the ontology-based activity estimation in the kitchen as an example. They also introduced the Dempster–Shafer theory of evidence [13] for addressing uncertainty between human behavior and the sensor outputs, and demonstrated the human activity estimation from the sensor outputs. It is interesting to note that their ontology network approach with the Dempster–Shafer theory has the potential to establish the standardization/generalization of the analyses from outputs of SBSs that are properly placed in the house.

In the sensing systems mentioned above, however, physiological measurement techniques have not been employed successfully to obtain such vital signs as ECG, body temperature and blood pressure. Nevertheless, directly relevant advances in physiological measurement techniques, with apparatus installed in household equipment, have been reported [14]–[20]. The development of these systems has arisen from the need for healthcare at home and is an independent approach to the smart home-based development. The main focus has been to design systems to monitor physiological variables in a fully automated manner, without the need either to attach any biological sensors to the body or for individuals to carry out any operations, simply using home facilities such as a bed, a bathtub, and a rest room. Similar to the concept of the smart home, the techniques used in the physiological measurement approach do not disturb normal daily activities, and thus the monitoring is done in an unconstrained manner, so-called "non-conscious physiological monitoring." This means that a subject does not need to be aware of the measurement being made, and the physiological data collected and stored are truly representative of normal daily living. In fact, this concept could also be applicable and useful for patient monitoring in a hospital room [17], [20].

With the nonconscious physiological monitoring system during sleeping the array of sensors incorporated within the bed can collect useful physiological data. This includes the cardiac pulse, respiration and snoring using a flat-type under-pillow sensor with vinyl tubes filled with silicone oil [17]–[20]. Also derived are a body surface contact-pressure distribution map together with body movements using a bed sheet-type pressure sensor with 2D-distributed multi-pressure elements [20]. For the care of the elderly there is a risk of drowning in the bathtub and a reliable alarm is needed. Therefore the bathtub monitoring system allows the simultaneous detection of the ECG together with respiration signals from electrodes embedded into the wall of the bathtub.

In the toilet monitoring system a highly accurate weighing scale device is installed in the lavatory floor around the toilet bowl. This is able to measure body and excretion weight and urination rate together with the ballistocardiogram (a small body weight change produced by cardiac blood ejection; [14], [15], [21]). Also, a system built into the toilet seat allows the blood

pressure to be measured [16], [17], [20]. Just recently, these authors have developed a network system that connects with each facility monitoring system using a Local Area Network (LAN). This network system is also supervised from another site (data server center) *via* a public Wide Area Network (WAN) with appropriate security, so as to consolidate individual healthcare information [20].

IV. Summary and Future Aspects of the Smart Home

The emergence and recent developments of the smart home have been briefly introduced in this review. Initial developments of smart homes comprised of computer-based housing to support elderly and challenged persons at home during daily living through the automatic monitoring of the usage of home infrastructures. In light of the rapid growth of the aging society, which has created what might be regarded as a longevity crisis, healthcare is also one of the most serious and worldwide issues to address. From this background, the smart home with healthcare management has rapidly been pushed into the spotlight.

Utilizing ICT technologies could also dramatically facilitate this approach, with the prospects of achieving smart home healthcare in an integrated manner [22], [23]. For example, Yuce [24] showed a very promising implementation approach for healthcare monitoring systems using W-BAN (wireless body area network). In addition, the smart home with ICT technologies has strong potential to realize fully a human support system including healthcare both in- and out of the house [18]–[20], [25], that is, to achieve a ubiquitous bioinstrumentation human support system (u-BHS).

To promote such u-BHS further, the establishment of an appropriate social infrastructure that meets the needs of human life support is urgently needed. Efforts to produce much more human-friendly and universally accepted u-BHSs, where a number of practical problems still remain, are likely to be resolved through the recent dramatic advances in the integration of microelectronic, micromechanical as well as ICT technologies.

Acknowledgment

The author wishes to thank Dr. M. Ogawa, Kanazawa University, for his elaborate efforts on assisting in the survey of publications relating to current smart home issues. He is also grateful to Professor P. Rolfe, Harbin Institute of Technology, China, and OBH Ltd., UK., for his help in preparing the manuscript.

References

[1] , M. A. Al-Qutayri, Ed., *Smart Home Systems*. Vukovar, Croatia: In-Tech, 2010, pp. 1–16.

[2] M. Weiser, "The computer for the 21st century," *Scientific Amer.*, vol. 265, no. 3, pp. 66–75, 1991.

[3] Production of a Roadmap for an Integrated Set of Standards for Smarthouse and Systems Related to it and an Open Event CENELEC, 2008 [Online]. Available: ftp://ftp.cencenelec.eu/CENELEC/SmartHouse/SmartHouseRoadmap.pdf

[4] M. Chan, E. Campo, D. Estève, and J. Y. Fourniols, "Smart homes—Current features and future perspectives," *Maturitas*, vol. 64, no. 2, pp. 90–97, 2009.

[5] P. N. T. Wells, "Can technology truly reduce health care costs?," *IEEE Eng. in Med. and Biol. Mag.*, vol. 22, no. 1, pp. 20–25, 2003.

[6] D. Ding, R. A. Cooper, P. F. Pasquina, and L. Fici-Pasquina, "Sensor technology for smart homes," *Maturitas*, vol. 69, no. 2, pp. 131–136, 2011.

[7] M. Skubic, G. Alexander, M. Popescu, M. Rantz, and J. Keller, "A smart home application to eldercare: Current status and lessons learned," *Technology and Health Care*, vol. 17, no. 3, pp. 183–201, 2009.

[8] Independent living by Americare & The Sinclair School of Nursing TigerPlace, 2011 [Online]. Available: http://www.americareusa.net/independent_living/Columbia_MO/zip_65201/americare/1335

[9] D. Heise, L. Rosales, M. Skubic, and M. J. Devaney, "Refinement and evaluation of a hydraulic bed sensor," in *Proc. 33rd Annu. Int. Conf. IEEE Eng. Med. Biol.*, 2011, pp. 4356–4360.

[10] M. W. Raad and L. T. Yang, "A ubiquitous smart home for elderly," *Info. Syst. Front.*, vol. 11, no. 5, pp. 529–536, 2009.

[11] J. Neuhaeuser, J. Diehl-Schmid, and T. C. Lueth, "Evaluation of a radio based ADL interaction recognition system in a day hospital for old age psychiatry with healthy probands," in *Proc. 33rd Annu. Int. Conf. IEEE Eng. Med. Biol.*, 2011, pp. 1814–1818.

[12] X. Hong, C. Nugent, M. Mulvenna, S. McClean, B. Scotney, and S. Devlin, "Evidential fusion of sensor data for activity recognition in smart homes," *Pervasive and Mobile Computing*, vol. 5, no. 3, pp. 236–252, 2009.

[13] G. Shafer, *A Mathematical Theory of Evidence*. Princeton, NJ: Princeton Univ. Press, 1976.

[14] K. Yamakoshi, M. Kuroda, S. Tanaka, I. Yamaguchi, and A. Kawarada, "Non-conscious and automatic acquisition of body and excreta weight together with ballistocardiogram in a lavatory," in *Proc. 18th Annu. Int. Conf. IEEE Eng. Med. Biol.*, 1996, pp. 10–11.

[15] K. Yamakoshi, "Unconstrained physiological monitoring in daily living for health care," *Front. Med. & Biol. Eng.*, vol. 10, no. 3, pp. 239–259, 2000.

[16] S. Tanaka, M. Nogawa, and K. Yamakoshi, "Fully automatic system for monitoring blood pressure from a toilet-seat using the volume-oscillometric method," in *Proc. 27th Annu. Int. Conf. IEEE Eng. Med. Biol.*, 2005, pp. 3939–3941.

[17] K. Motoi, M. Ogawa, H. Ueno, Y. Kuwae, A. Ikarashi, T. Yuji, Y. Higashi, S. Tanaka, T. Fujimoto, H. Asanoi, and K. Yamakoshi, "A fully automated health-care monitoring at home without attachment of any biological sensors and its clinical evaluation," in *Proc. 31st Annu. Int. Conf. IEEE Eng. Med. Biol.*, 2009, pp. 4323–4326.

[18] K. Yamakoshi, "Current status of non-invasive bioinstrumentation for healthcare," *Sens. and Mater.*, vol. 23, no. 1, pp. 1–20, 2011.

[19] K. Motoi, A. Ikarashi, S. Tanaka, and K. Yamakoshi, "Ubiquitous healthcare monitoring for daily life," in *Distributed Diagnosis and Home Healthcare*, U. R. Acharya, Ed. *et al.* Valencia, CA: American Scientific, 2011.

[20] K. Motoi, S. Taniguchi, T. Yuji, M. Ogawa, N. Tanaka, K. Hata, M. Baek, H. Ueno, M. Wakugawa, T. Sonoda, S. Fukunaga, Y. Higashi, K. Matsumura, T. Yamakoshi, S. Tanaka, T. Fujimoto, H. Asanoi, and K. Yamakoshi, "Development of a ubiquitous healthcare monitoring system combined with non-conscious and ambulatory physiological measurements and its application to medical care," in *Proc. 33rd Annu. Int. Conf. IEEE Eng. Med. Biol.*, 2011, pp. 8211–8214.

[21] K. Yamakoshi, "In the spotlight: Bioinstrumentation," *IEEE Rev. Biomed. Eng.*, vol. 2, pp. 2–5, 2009.

[22] C. Chen and C. Pomalaza-Raez, "Implementing and evaluating a wireless body sensor system for automated physiological data acquisition at home," *Int. J. Comput. Sci. Info. Technol.*, vol. 2, no. 3, pp. 24–38, 2010.

[23] H. Huo, Y. Xu, H. Yan, S. Mubeen, and H. Zhang, "An elderly health care system using wireless sensor networks at home," in *Proc. 3rd Int. Conf. Sensor Technologies and Applicat.*, 2009, pp. 158–163.

[24] M. R. Yuce, "Implementation of wireless body area networks for healthcare systems," *Sens. Actu. A: Physical*, vol. 162, no. 1, pp. 116–129, 2010.

[25] J. Kim, S. Cho, and S. J. Kim, "Preliminary studies to develop a ubiquitous computing and health-monitoring system for wheelchair users," in *Proc. 3rd Int. ICST Conf. Body Area Netw.*, 2008, doi: 10.4108/ICST.BODYNETS2008.2974.